Synthesis of Metal oxides/sulfides and porous Carbon for energy storage application.

A Thesis Submitted towards Partial Fulfillment of

BS-MS Dual Degree Program

By

Kush Kumar Upadhyay

Under the Guidance of

Prof. S.B Ogale, NCL Pune, India

And

Dr. Seema Verma, IISER Pune, India

Department of Chemistry

Indian Institute of Science Education and Research (IISER) Pune

Dedicated To My

Parents

And Teachers

Certificate

This is to certify that this dissertation entitled "**Synthesis of Metal oxides/sulfides and porous Carbon for energy storage application.**" towards the partial fulfillment of the BS-MS dual degree program at the Indian Institute of Science Education and Research Pune, represents original research carried out by **Kush Kumar Upadhyay** at Department of physical and materials chemistry, National Chemical Laboratory (NCL) Pune under the supervision of **Prof. Satishchandra B. Ogale**, NCL, Pune during the academic year 2013-2014.

Kush Kumar Upadhyay

Prof. S.B Ogale
(Supervisor)

Date:

Place: **Pune**

Prof. K.N. Ganesh
(Head of Chemistry department)

Date:

Place: **Pune**

Declaration by the Candidate

I declare that the thesis entitled "**Synthesis of Metal oxides/sulfides and porous Carbon for energy storage application**" submitted by me for the degree of Master of Science for the record of work carried out by me during the academic year 2013-2014 at Department of Physical and Materials chemistry under the guidance of **Prof. Satishchandra B. Ogale**, NCL Pune. This work has not formed the basis for the award of any degree, diploma, and fellowship, titles in this or any other University or other institution of higher learning. I further declare that the material obtained from other sources has been duly acknowledged in the thesis.

Kush Kumar Upadhyay

DATE:
PLACE: PUNE

Acknowledgements

Foremost, I would like to express my sincere heartfelt gratitude to my guide **Prof. Satishchandra B. Ogale** for providing me with an opportunity to work for my master's thesis. I am always indebt for his continuous motivation, encouragement, scientific advice, support and co-operation during the course of this work. I also express my gratitude towards **Dr. Seema Verma** for supporting me as my local co-ordinator at IISER, Pune and also her for motivation which helped me complete the task.

I would like to thank, **Prof. K. N. Ganesh**, Director of Indian institute of Science Education & Research, for allowing the thesis work to be carried out National Chemical Laboratory, Pune.

Besides that I would like to give my sincere thanks to **Mr. Abhik Banerjee**, **Mr. Rohan Gokhale, Mr. Onkar Game** and **Mr. Wahid Malik** for their insightful comments, hard questions, encouragement, their guidance and helping in using experimental tools in the very beginning of my work.

I would also like to thank all my labmates and friends Dhanya, Vishal, Satish, Reshma, Shruti, Dr. Lily Mandal, Dr. Mandakini Biswal, Dr. Dattakumar Mhamane, Shraddha, Pradeep, Pooja, Anil, Aniruddha, Dr.Parvez Shaikh, Dr.Sarika Phadke, Mukta, Umesh, Ketaki, Upendra, Sumit, Akash and Tanya for providing an academically exciting atmosphere.

Lastly I would like to thank my friends Montu, Vikas, Dinesh, Ashok, Zoheb, Abhishek Kumar, Abhishek Singh, Pramod, Meena, Sher singh, Rajkumar, Anurag agrawal and Vivek kumar for being with me in my bad times and for their encouragement during this work.

---Kush Kumar Upadhyay

Contents

List of Abbreviations

0D	Zero Dimensional
1D	One Dimensional
2D	Two Dimensional
3D	Three Dimensional
BET	Brunauer Emmett Teller
CNT	Carbon Nanotube
CV	Cyclic Voltammetry
CNF	Carbon Nano Fiber
D.I.	De Ionized
ED	Electron Diffraction
EDL	Electric Double Layer
EDLC	Electrochemical Double Layer Capacitor
EIS	Electrochemical Impedance Spectroscopy
ES	Electrochemical Supercapacitor
ESR	Equivalent Series Resistance
EV	Electric Vehicles
FCs	Fuel Cells
FESEM	Field Emission Scanning Electron Microscope
HEV	Hybrid Electric Vehicles
HRTEM	High Resolution Transmission Electron Microscope
LIB	Lithium ion battery
Li-HEC	Lithium ion hybrid electrochemical capacitor
MOF	Metal Organic Framework
MOF-DC	Metal Organic Framework derived Carbon
NPs	Nanoparticles
NCO	Nickel Cobalt Oxide
NCS	Nickel Cobalt Sulfide
SC	Supercapacitor
SEM	Scanning Electron Microscope

List of Figures

Chapter 1

Chapter 2

Chapter 3

Chapter-1

Introduction on Supercapacitors.

By seeing the rapid development of the global economy, the rapid rate of depleting fossil fuels, and increasing environmental pollution, there is an urgent need for efficient, environmental friendly and sustainable sources of energy as well as new technologies associated with energy conversion and storage.

Energy stored as potential energy is involved in hydroelectric systems through the hydrostatic “head” of water behind dams; it is also stored in a potential sense in fuels (e.g. coal, oil and cryogenic hydrogen) and becomes available, albeit with rather poor efficiency, through combustion utilizing steam-piston, steam turbine and internal combustion engines of various kinds as energy transduction devices. But now to fulfill the increasing demand of energy some of the most effective and practical technologies for electrochemical energy conversion and storage has been investigated and these are batteries, fuel cells, and electrochemical supercapacitors (ES). In recent years, ES or ultracapacitors have attracted significant attention, mainly due to their high power density, long lifecycle, and bridging function for the power/energy gap between traditional dielectric capacitors (which have high power output) and batteries/fuel cells (which have high energy storage).[1,2]

Electrochemical supercapacitors was first introduced in 1957. At that time it was thought that this kind of ES could only be used to boost up the functioning of battery or fuel cell in a hybrid electric vehicle to provide the necessary power for acceleration.[3] But further developments have led to recognition that ES can act as superior energy storage device than that of battery in many respects (**fig. 1**). As a result the US Department of Energy has designated ES to be as important as batteries for future energy storage systems.[4] Many other industries and enterprises have also taken interest in it and have started investing money into exploring, researching, and developing ES technologies. Recently this area have drawn a wide attention which have resulted in progress of both

theoretical and practical research and development of electrochemical supercapacitors.[5-13] The major challenge in this field before scientific community today is its low energy density and high production cost.

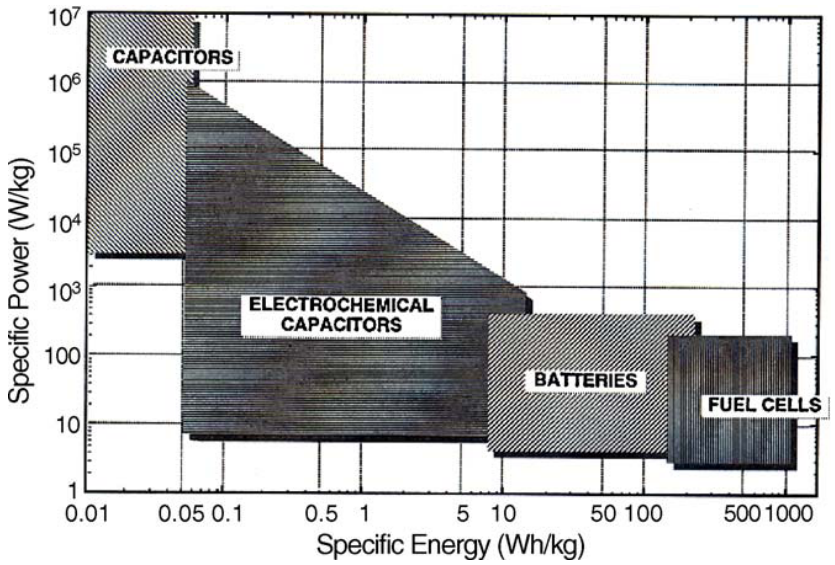

Figure 1. Specific energy and power capabilities of capacitors (electrostatic), electrochemical capacitors (supercapacitors), batteries and fuel cells.

In order to overcome the low energy density problem in case of ES there must be intensive approaches in synthesis of novel electrode materials for ES electrodes. There are various materials investigated showing the better charge storage properties. Most popular today are carbon particle materials having very high active surface area. But in spite of its high surface area it has limited specific capacitance because the physical adsorption of ions in the pores of carbon are limited which also finally limits the energy density. Therefore various other materials other that carbon have been also investigated like metal oxides and their composites which shows faradaic nature and also shows very enhanced energy density. The advantage of using metal oxides as electrode active material is that they not only allow ions to get adsorbed on the surface but also facilitates in redox reaction at electrode-electrolyte interphase which increases the capacitance by several times compaired to carbon based materials (Metal oxides such as ruthenium oxides and manganese oxides are considered the most promising

material for the future ES.)[14-16] but the problem with the metal oxides based material is cyclability. To overcome with this problem and to enhance the energy density, composite based material has been widely investigated named as hybrid double layer supercapacitors.

1.1 Fundamentals and applications of supercapacitors

Like batteries electrochemical-supercapacitors are energy storage similar in design and manufacturing. The main components of ES are two electrodes, an electrolyte and a separator that electrically isolates the two electrodes. The most important component among them is the electrode material which governs its specific capacitance. For an efficient supercapacitor the electrode materials are required to possess:

- high specific surface area, which governs the specific capacitance,
- controlled porosity, which affects the the specific capacitance and the rate capability,
- high electronic conductivity , which is crucial to the rate capability and the power density,
- desirable electroactive sites, which enable pseudocapacitance,
- high thermal and chemical stability which effect the cyclic stability, and
- low costs of raw materials and manufacturing.

This is because electrical double-layer capacitors (EDLCs), store charge by adsorption of electrolyte ions onto the surface of electrode materials. On applying the opposite potential to both the electrodes, the cations moves towards the negatively charged electrode and anions moves towards the positively charged electrode and get adsorbed physically on the surface of the electrode as can be seen in the **figure 2**. This forms an interphase between electrode and electrolyte which can be treated as a capacitor having capacitance expressed by equation (1):

$$C = \frac{A \in}{4\pi d} \qquad (1)$$

where A is the active surface area of the electrode, ∈ is the dielectric constant of the medium which varies depend on the medium like 1 for vacuum and larger than 1 for all other materials, including gases; and d is the effective thickness of the electric double layer.

As introduced earlier supercapacitors store energy via two different mechanisms. The first one is electrochemical double layer supercapacitor in which only the physical adsorption/desorption of the electrolytic ions takes place on the surface of electrode on applying potential in a complete reversible manner. The second one is pseudo-capacitance in which the electrolyte ions undergo redox reaction at the surface of the electrode material.

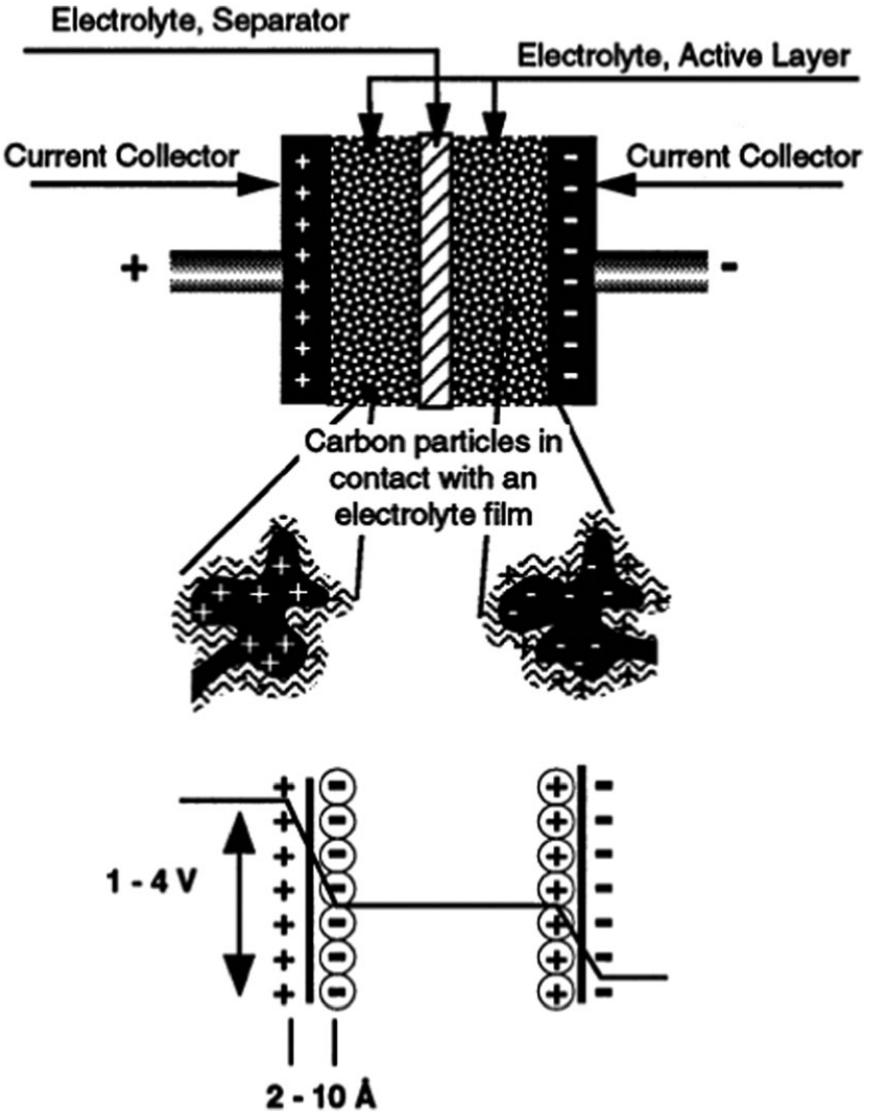

Figure 2. Principles of a single-cell double-layer capacitor and illustration of the potential drop at the electrode/electrolyte interface.

1.2 Electrochemical double layer supercapacitors (EDLS)

In EDLS, the electrostatic charge accumulation on the surface of ideally polarizable electrode is potential dependent. Generally three different zones of charge accumulation have been defined based on the distance from the surface of the electrode. On applying potential the double layer formation takes place. One layer forms in the surface lattice structure of the electrode. The other layer with opposite polarity emerges from the dissolved and solvated ions from the electrolyte. These two layers are basically separated by a monolayer of solvent molecules like water.

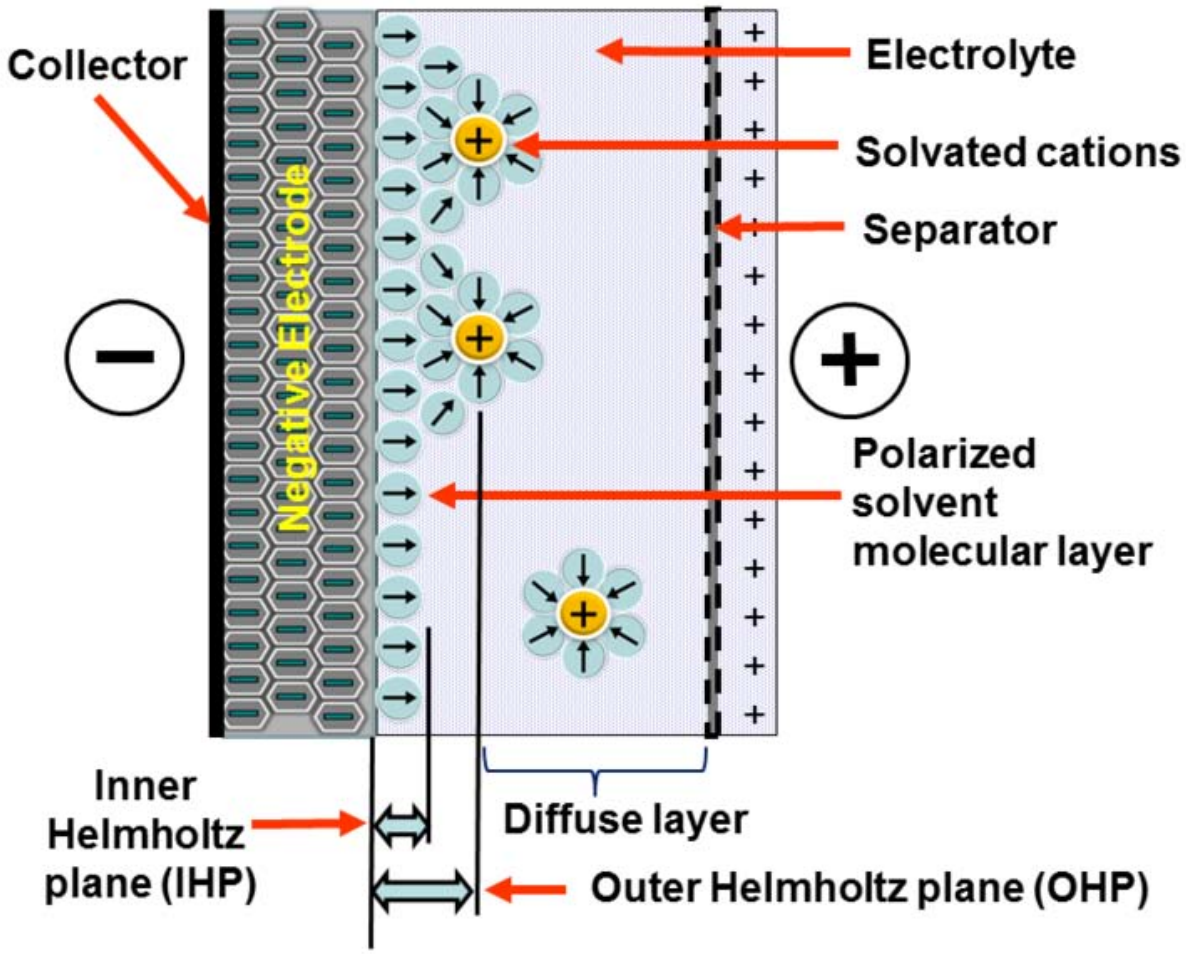

Figure 3. Schematic diagram showing EDLS mechanism.

This monolayer forms the inner Helmholtz plane which adheres to the surface of electrode and separates the appositively charged ions, acting as molecular dielectric. The physical forces not the chemical forces cause the adhesion of the solvent. The amount of charge in outer Helmholtz plane (OHP) matches with the charge in the electrode. After the OHP there is diffused layer of counter ions exist in the electrolyte as you can see in **figure 3**. During the process of charging the electrons flow from the negatively charged electrode to positively charged electrode through an external load. And within the electrolyte cations moves towards the negatively charged electrode and anions move towards positively charged electrode and the reverse process happens on discharging of supercapacitors. Since the electrode used in the EDLS is ideally polarizable electrode so no any charge transfer takes place between electrode-electrolyte interphase as well as no net ion exchanges take place between the electrode and electrolyte. This means that the concentration of electrolyte remains constant in this mechanism of charge storage. In this way energy is stored in EDLS system.

If the two electrode surfaces can be expressed as E_{S1} and E_{S2}, an anion as A^-, a cation as C^+, and the electrode/electrolyte interface as //, the electrochemical processes for charging and discharging can be expressed as:[17,18]

On positive electrode:

$$E_{S1} + A^- \xrightarrow{\text{charging}} E^+_{S1}// A^- + e^-$$

$$E^+_{S1}// A^- + e^- \xrightarrow{\text{discharging}} E_{S1} + A^-$$

On the other hand on negative electrode:

$$E_{S2} + C^+ + e^- \xrightarrow{\text{charging}} E^-_{S2}// C^+$$

$$E^-_{S2}// C^+ \xrightarrow{\text{discharging}} E_{S2} + C^+ + e^-$$

Overall charging and discharging can be expressed as:

$$E_{S1} + E_{S2} + A^- + C^+ \xrightarrow{\text{charging}} E^+_{S1}// A^- + E^-_{S2}//C^+$$

$$E^+_{S1}// A^- + E^-_{S2}//C^+ \xrightarrow{\text{discharging}} E_{S1} + E_{S2} + A^- + C^+$$

1.3 Faradaic supercapacitors

The ideal non-polarizable electrode shows faradaic supercapacitive nature. These types of supercapacitors are also named as pseudocapacitor. On applying the potential to this type of supercapacitor the ions get selectively adsorbed on the electroactive site and undergoes fast and reversible faradaic reaction (redox reaction) on the surface of the electrode and involve the passage of charge across the double layer in similar way as happens in the batteries. There are three different kinds of faradaic mechanism takes place at the surface of electrode: reversible adsorption (e.g. adsorption of hydrogen on the surface of electrode, redox reactions of transition metal oxides and reversible electrochemical doping-dedoping in conducting polymer based electrodes. The magnitude of pseudocapacitance can be expressed by equation:

$$C = \frac{n \times F}{M \times V} \qquad (2)$$

Where n is the mean number of electrons transferred in the redox reaction, F is the faraday constant, M is the molar mass of metal oxides and V is the operating potential window.

The chief materials showing pseudocapacitive behaviour are conducting polymers and several binary and ternary metal oxides like RuO_2, MnO_2, and Co_3O_4.[14, 19-21]It has been observed that in the case of faradaic supercapacitor the working potential window increases in comparison to EDLS which result in the enhancement of energy density as well as capacitance by several factors.[22] This is because in case of FS the electrochemical process occurs both at surface as well as bulk near the surface of solid electrode. As reported by Conway *et al*.[23] the capacitance of FS can be 10-100 times higher than the electrostatic capacitance of an EDLS. But on compairing the power density of FS and EDLS, FS has relatively low because faradaic processes are normally

slower than non-faradaic processes.[24] Also FS generally lacks stability during cycling because of continuous going redox reaction at electrode-electrolyte interphase.

Asymmetric supercapacitor has drawn a wide attention in this field. This is because in this we can club both the EDLS and FS electrode properties which will enhance the overall cell potential resulting in overall increment of energy density and power density.[13, 25, 26]

1.4 ES capacitance, voltage, power and Energy density

Fig. 2 clearly shows that there are two capacitors connected in series. Let say, the capacitance of positive electrode be C_p and negative electrode be C_n then the overall capacitance (C_T) of the cell can be expressed as equation: [10]

$$1/C_T = 1/C_P + 1/C_n \qquad (3)$$

In the case of symmetric supercapacitors, $C_p = C_n$ and so the overall capacitance, C_T, is half of either one's capacitance. But when $C_p \neq C_n$, this usually happens when the anode and cathode have different materials, then the C_T is generally dominated by the one with smaller capacitance value. These types of supercapacitors are known as asymmetric supercapacitor.

On charging the electrochemical supercapacitors, potential (V) is build up across two electrodes. And the energy and power density of supercapacitors depend directly on the square of the potential which can be expressed by the equations given below: [6, 7]

$$\boldsymbol{E = \frac{CV^2}{2} = \frac{QV}{2}} \qquad \boldsymbol{(4)}$$

$$\boldsymbol{P = \frac{V^2}{4R_S}} \qquad \boldsymbol{(5)}$$

Where Q denotes the total charge stored in the electrochemical supercapacitor and R_S denotes the equivalent series resistance of the ES. From these two equations it can be concluded that the performance of ES is manly dependant on three variable parameters i.e. *V, C* and R_S. So in order to enhance the energy and power density one has to put effort in increasing the values of both V and C and reducing the value of R_S. The working potential window depends basically on the type of materials used for making electrode and the type of electrolyte. For example when carbon is used as electrode in aqueous medium its potential window is restricted between 0-1 V while in organic electrolyte the potential window is in the range of 0-3 to 3.5V. The electrolyte's stability also determines the electrode working potential window. Since the above equations indicate that both energy density and power density are proportional to the square of the square of voltage, therefore increasing the working potential window may be more effective than increasing capacitance or reducing inner resistance in terms of raising the ES's energy and power density. To increase the ES's cell voltage within the electrolyte's stability window, selecting the type of electrode materials and optimizing electrode structures can achieve high cell voltages.

Equation (4) indicates that the energy density of ES is directly related with the capacitance value. Therefore energy density value can be improved with the improvement of capacitance value. Optimizing electrode layer structures, the capacitance value can be enhanced. Therefore, developing electrode materials should be one of the key approaches in ES research and development.

Furthermore, eqn (5) indicates how the cell resistance depends on the internal resistance of the supercapacitor. In order to increase the power density, the overall cell resistance should be decreased. The cell resistance is a sum of electrode and electrolyte resistances (i.e. charge transfer resistance at electrode-electrolyte interphase, ionic resistance because of their movement in electrolyte and electronic resistance in the electrode), should be the major focus. Generally, ES's have lower internal resistance compared with the Li ion batteries therefore supercapacitor possesses high power density than batteries. The performance of an electrode material is defined after measuring its specific capacitance. The specific capacitance is the

intrinsic capacitance of the material expressed in Faraday per gram (F g^{-1}) and it is obtained by equation given below:

$$C_S = \frac{C_i}{W} \qquad (6)$$

Where W is the weight of the electrode materials in the electrode layer in grams and C_i is the electrode capacitance (anode or cathode). Here it should be clearly noted that higher specific capacitance of a material does not mean that it will be a good electrode material. This is because the capacitance of supercapacitors also strongly depends on the morphology of the electrode like layered structure, 1-D nanorods, sheet etc so that most of the surface area get exposed to the electrolyte and the electrons and ions mobility should be accessible within the layers. This is because the coating of extremely thin layer of the electrode material on the substrate will give you very high specific capacitance value because as you can see in equation 6 that loading is inversely proportional to specific capacitance. But in real case when we go for fabricating electrode for real supercapacitor application, we coat thick layer on the electrode for maximum energy density but problem faced in that case is low capacitance value from expected value.

1.5 The Role of Electrolyte

Electrolyte plays the most important role in the performance of electrochemical supercapacitor. The energy density of supercapacitor also depends on the type and performance of electrolyte. Therefore an ideal electrolyte to have better performance it should have properties like to work for wide operating potential window, high electrochemical stability, high ionic concentration, low solvated ionic radius, low resistivity, low viscosity, low volatility, low toxicity, low cost and easier avaibility. The electrolytes used in supercapacitors are classified into three different types:

1) Aqueous electrolyte: Electrochemical supercapacitors give better performance in aqueous electrolyte like H_2SO_4, KOH, Na_2SO_4, NH_4Cl etc. because of their higher ionic concentration and smaller ionic radius. The advantage of smaller ionic radius of these electrolytes are they experience very low resistance when

the counter ions moves towards oppositively charged electrode on applying potential which reduces equivalent series resistance by various factors. This results in higher power density as well as higher capacitance value. The major disadvantage in using aqueous based electrolyte is its narrow working potential window only upto 1.2 V, much lower than that of organic electrolyte. The eqn (4) and (5) say that the energy and power density both depends on potential window which is restricted only upto 1.2 V in case of aqueous electrolyte. This is the reason why organic electrolytes are recommended.

2) Organic electrolyte: Organic electrolytes have larger potential window upto 3.5 V compaired to aqueous electrolytes. This is the major advantage of organic electrolyte over aqueous electrolytes. The most common solvent used as organic electrolyte are acetonitrile and propylene carbonate (PC). Acetonitrile can dissolve larger amounts of salts but suffers from environmental and toxic problems. The benefit of using PC- based electrolyte is its high operating potential window, a wide range of operating temperature, possesses good conductivity as well as environmentally friendly. There are various other organic salts used as ES electrolyte like tetraethylammonium tetrafluoroborate, tetraethylphosphonium tetrafluoroborate and triethylmethylammonium tetrafluoroborate ($TEMABF_4$). One thing that should be kept in mind is that the water content in organic electrolyte must be kept below 3-5 ppm otherwise the ES's voltage will be significantly reduced.

1.6 References

1. C. Largeot, C. Portet, J. Chmiola, P. Taberna, Y. Gogotsi and P. Simon, J. Am. Chem. Soc., **2008**, 130, 2730.

2. S. Kandalkar, D. Dhawale, C. Kim and C. Lokhande, Synth Met., **2010**, 160, 1299.

3. R. Ko¨ tz, S. Mu¨ ller, M. Ba¨ rtschi, B. Schnyder, P. Dietrich, F. N. Bu¨ chi, A. Tsukada, G. G. Scherer, P. Rodatz, O. Garcia, P. Barrade, V. Hermann and R. Gallay, Electrochem. Soc. Proc., **2001**, 21, 564.

4. P. Simon and Y. Gogotsi, Nat. Mater., **2008**, 7, 845.

5. E. Frackowiak, Phys. Chem. Chem. Phys., **2007**, 9, 1774.

6. L. Zhang and X. S. Zhao, Chem. Soc. Rev., **2009**, 38, 2520.

7. H. Pan, J. Li and Y. Feng, Nanoscale Res. Lett., **2010**, 5, 654.

8. M. Inagaki, H. Konno and O. Tanaike, J. Power Sources, **2010**,195, 7880.

9. E. Frackowiak and F. Beguin, Carbon, **2001**, 39, 937.

10. A. G. Pandolfo and A. Hollenkamp, J. Power Sources, **2006**, 157, 11.

11. P. Simon and A. Burke, Interface, **2008**, 17, 38.

12. S. W. Zhang and G. Z. Chen, Energy Mater., **2008**, 3, 186.

13. A. Burke, J. Power Sources, **2000**, 91, 37.

14. B. E. Conway, Electrochemical Supercapacitors, Kluwer Academic/Plenum Press, New York, 1999.

15. B. Babakhani and D. G. Ivey, Electrochim. Acta, **2010**, 55, 4014.

16. S. Sarangapani, B. V. Tilak and C. P. Chen, J. Electrochem. Soc. **1996**, 143, 3791**.**

17. J. P. Zheng, J. Huang and T. R. Jow, J. Electrochem. Soc., **1997**, 144, 2026.

18. Y. M. Vol'fkovich and T. M. Serdyuk, Russ. J. Electrochem., **2002**, 38, 935.

19. M. S. Wu and P. C. Chiang, Electrochem. Solid-State Lett., **2004**, 7, A123.

20. W. Sugimoto, H. Iwata, Y. Murakami and Y. Takasu, J. Electrochem. Soc., **2004**, 151, A1181.

21. X. Dong, W. Shen, J. Gu, L. Xiong, Y. Zhu, H. Li and J. Shi, J. Phys. Chem. B, **2006**, 110, 6015

22. Y. Zhang, H. Feng, X. Wu, L.Wang, A. Zhang, T. Xia, H. Dong, X. Li and L. Zhang, Int. J. Hydrogen Energy, **2009**, 34, 4889.

23. B. E. Conway, V. Birss and J. Wojtowicz, J. Power Sources, **1997**, 66, 1.

24. C. Ming Chuang, C. W. Huang, H. Teng and J. M. Ting, Energy Fuels, **2010**, 24, 6476.

25. M. Kisacikoglu, M. Uzunoglu and M. Alam, Int. J. Hydrogen Energy, **2009**, 34, 1497.

26. S. Ma, K. Nam, W. Yoon, X. Yang, K. Ahn, K. Oh and K. Kim, Electrochem. Commun., **2007**, 9, 2807.

Chapter 2

$NiCo_2S_4$ nanowires array supercapacitor on carbon fiber paper.

2.1 Abstract

In this chapter I will discuss about a novel synthetic protocol that involves direct growth of ternary nickel cobalt sulfide ($NiCo_2S_4$) nanowires (NCS NWs) on a carbon fiber paper for high performance supercapacitor application. NCS NWs were synthesized by wet chemical sulfurization of nickel cobalt oxide ($NiCo_2O_4$) nanowires (NCO NWs) using Na_2S as a sulfurization agent. The synthesized NCS NWs have a hierarchical morphology, and a direct electrical contact with the porous, conducting and stable carbon fiber paper substrate. The material exhibits a maximum areal capacitance of 2.65 F/cm^2 at a current density of 1 mA/cm^2 (which is around six times higher than that of NCO NWs) and a gravimetric capacitance 2027 F/g at the current density of 4.8 A/g, with a high rate capability (40% capacitance retention at a current density of 40 mA/cm^2). We demonstrate and discuss the rich redox chemistry of the NCS NWs in comparison to its NCO counterpart.

2.2 Introduction

The growing energy demand brought about by extensive requirement and use of different electronic devices has motivated researchers to pursue high performance advanced electrode materials for charge storage applications.[1,2,3] Owing to its unique characteristics of high power density, superior pulse charge/discharge, long cycle life and environmental friendliness for use in portable systems and hybrid vehicles, the supercapacitor is easily one of the most attractive options among all the charge storage systems for these applications. Based on the electrode material used, supercapacitors exhibit two types of charge storage mechanisms, namely the Electrical Double Layer Capacitance (EDLC) mechanism which operates through the adsorption of ions at the

electrode-electrolyte interface by Coulombic attractive forces and the Pseudo-capacitance mechanism which involves a fast reversible redox reaction at the electrode-electrolyte interface with a faradic transfer of electrons.[4] Low cost and chemically inert porous carbon materials that possess high surface area and good electronic conductivity have been employed as electrode materials for EDLC type devices. However, despite several efforts there are certain limitations on their achievable capacitance values resulting in devices with low energy densities. [5-7] This factor restricts the usage of EDLC based systems in several applications. Alternatively, pseudo-capacitive materials offer much higher specific capacitance than EDLCs but with unsatisfactory cyclability and low stability. For example, though hydrous RuO_2 is one of the best-performing pseudo-capacitive electrode materials demonstrating high specific capacitance, high conductivity and long term cyclability, its toxic nature and high cost render it unsuitable for practical commercial applications. In light of these facts, current research on supercapacitors is directed towards development/synthesis of high performance, stable, inexpensive, and non-toxic electrode materials for pseudo-capacitive devices. [8]

One-dimensional nanostructured materials are favorable for pseudo-capacitive charge storage applications because of their high electro-active surface area which results in the utilization of the entire material content. Furthermore an oriented growth of one-dimensional nanostructures provides an access space for easy diffusion of ions resulting in improved charge transfer kinetics of the system. Moreover a much shorter mean electron diffusion length in these structures from the location of the surface reaction site lowers internal resistance of the electrode materials as well. [9,10]

Of all the binary transition metal oxides and sulfides, nickel and cobalt oxides/sulfides have been found to be the materials of choice with regard to their non-toxicity, low cost, and various suitable nanostructures for high specific capacitance values.[11-15] However, these binary systems suffer from a drawback of poor capacitance at high current densities, thereby incapacitating them for high rate charge storage applications. Based on this consideration, extensive work on the synthesis of pure phase ternary oxide

nanostructures is currently in progress for good performance in charge storage applications.[16, 17] Nickel cobalt oxide {$NiCo_2O_4$-(NCO)} is one such structurally tunable, electrochemically active ternary oxide with electronic conductivity higher by two orders of magnitude as compared to the binary oxide counterparts like NiO and Co_3O_4. A range of nanostructures including one-dimensional nanowire have been reported for NCO as an electrode material in supercapacitors. For example, Hu and coworkers reported the cost effective NCO aerogel with maximum specific capacitance of 1400 F/g[16] and Zhang et al. reported the specific capacitance of 1743.4 F/g at the current density of 8.5 mA/cm2.[17] Despite several reports on ternary NCO as a charge storage material, its corresponding sulfide; nickel cobalt sulfide {$NiCo_2S_4$-(NCS)} has remained largely unexplored. Very recently Chen et al.[18] synthesized ternary NCS and demonstrated its efficient capacitive performance. This work established the fact that NCS as a material exhibits richer redox chemistry as compared to its corresponding binary sulfides and possesses a major advantage over NCO in terms of higher electronic conductivity. However the only reported synthesis of NCS involves hydrothermal synthesis of the material in powder form with a three-dimensional urchin-like microstructure. Thus, further processing of NCS for making supercapacitor electrodes necessitates the formulation of a paste by addition of an insulating binder. This insulating polymer binder increases the resistance, cost and weight; factors which are counter-productive to the capacitive performance, although it has an advantage of enhancing volumetric capacitance. Therefore, it is indeed very useful to directly grow one dimensional nanostructures on a conductive substrate in order to generate an electrode for effective charge storage without the use of binders/additives.

In this work we report on a strategy towards the oriented growth of one dimensional NCS NWs by sulfurization of hydrothermally grown, vertically oriented NCO NWs directly on a conductive carbon substrate (Please see schematic of **Figure 1a** and the experimental section). Additionally, individual nanostructures synthesized by this process have a direct electrical contact with the conductive substrate via conducting channels, thereby enhancing the electron transfer kinetics. Of all the conductive substrates such as stainless steel, nickel foam, titanium foil, graphite, carbon

cloth/paper etc. used in supercapacitor devices, carbon fiber paper was chosen in this work because of its excellent characteristics of light weight, high conductivity, porosity and chemical inertness. [10, 19, 20] The SEM image of such substrate is shown in **Figure 1b**.

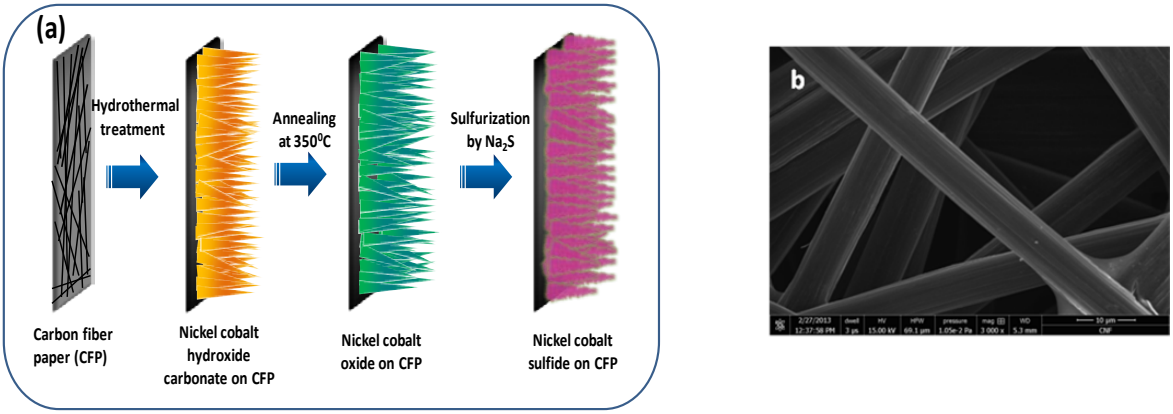

Figure 1(a) Schematic diagram of formation of NCS NWs: Step-I is the formation of metal oxide carbonate NWs by hydrothermal method, Step-II is the formation of NCO NWs by annealing in air for 2 hours, Step-III is the sulfurization process by wet chemical method using Na2S at 120°C for 36 hours ; (b) SEM image of the carbon fiber paper

2.3 Experimental section

Synthesis of NCO NWs:

Commercially available carbon fiber paper was washed with dilute (0.1M) H_2SO_4 followed by sonication with de-ionized water for 15 minutes prior to deposition. A 150 ml solution containing 2 mmol nickel nitrate hexahydrate, 4 mmol of cobalt nitrate hexahydrate and 10 mmol of urea was prepared and homogenized by sonication. The homogeneous solution was transferred to a 200 ml Teflon-lined stainless steel autoclave. A piece of washed carbon fiber paper was vertically immersed into the above solution. The autoclave was sealed and then transferred into an electric oven. The temperature of the oven was maintained at 120 °C for 19 hours. The carbon fiber paper was removed from the solution after cooling the autoclave at room temperature. The carbon paper supported nanowires array was washed with DI water and ethanol for several times and then annealed at 350 °C for 2 h for the synthesis of NCO NWs array.

The mass loading of the NCO NWs is 0.92 mg/cm^2.Synthesis of hierarchical NCS NWs The carbon paper supported nanowires array was kept in a 200 ml autoclave containing 100 ml solution of 10 mmol Na_2S. The autoclave was heated at 120 °C for different time periods (12 hrs, 24hrs and 36 hrs). After cooling down to room temperature, the NCS NWs array was washed in DI water and carbon disulfide for several times to remove the excess sulfur and dried overnight in a vacuum oven at 40 °C. The mass loading of the NCS NWs is 1.04 mg/cm^2. The complete procedure has been represented diagrammatically in the schematic of **Figure 1a**.

2.4 Electrochemical Measurements

Cyclic voltammetry (CV) studies, galvanostatic charge-discharge measurement and Electrochemical impedance analysis were carried out using three-electrode systems (carbon paper supported nanowires array used as working electrode, Hg/HgO as reference electrode and platinum strip as a counter electrode). Cyclic voltammetry was carried using 2M aqueous KOH solution as the electrolyte at different potential scan rates (1-8 mV/s). The potential window used in the measurement was from 0 to 0.55 volts. Charging and discharging was carried out galvanostatically by varying the current density from 1 mA/cm^2 to 40 mA/cm^2 over a potential range of 0-0.55 V. Cyclic stability was carried out by galvanostatic charge-discharge at a constant current density (20 mA/cm^2) up to 1000 cycles.

2.5 Characterizations

Field Emission Scanning Electron Microscopy (FESEM, Nova NanoSEM 450) and High Resolution-Transmission Electron Microscopy (HR-TEM, FEI Tecnai 300) were used for imaging and diffraction. X-ray Diffraction (XRD, Philips X'Pert PRO) was used for structural determination. Cyclic voltametry, galvanostatic charge discharge and Impedance measurements were done using AutoLab potentiostat with Nova 1.7.

2.6 Calculations

Areal and specific capacitance values were calculated from the charge-discharge measurement by the following equation:

$C_{sp} = (I \times t)/(\Delta V \times S)$

Where I is the constant discharge current, t is the discharging time, ΔV is the potential window (excluding the IR drop) and S is the geometrical surface area of the electrode. Electrochemical impedance spectroscopy (EIS) was carried out at the bias potential of 0.2V by applying Ac voltage in the frequency range of 0.01Hz - 10^5 Hz with amplitude of 5 mV in three electrode assembly.

2.7 Results and Discussions

The x-ray diffraction (XRD) patterns of the NCO and NCS NWs were obtained by scratching the coating from the carbon fiber paper. All the peaks can be attributed to different planes of their spinel cubic phase (**Figure 2**).[18, 20] (PCPDF-731702 for NCO and 431477 for NCS) The peak at 2θ value of 31.400 can be identified with the 311 plane of NCS with 100% intensity, whereas the peak position at 2θ values of 360 represents the 100 plane of NCO with 100% intensity.[21] No impurity phases are seen.

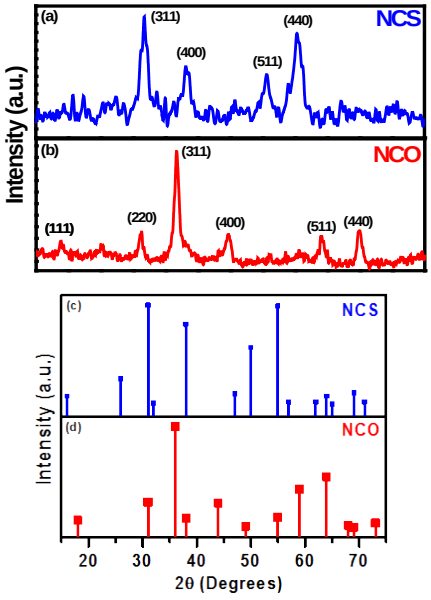

Figure 2 XRD patterns of the (a) NCS NWs and (b) NCO NWs. The expected locations of the peaks for the two phases based on PCPDF data are shown in (c and d**).**

Scanning electron microscopy (SEM) was employed to investigate the morphology as well as the nature of the surfaces. **Figure 1b** shows the SEM images of the carbon fiber paper where the well-connected carbon fibers with typical width of 5 μm can be

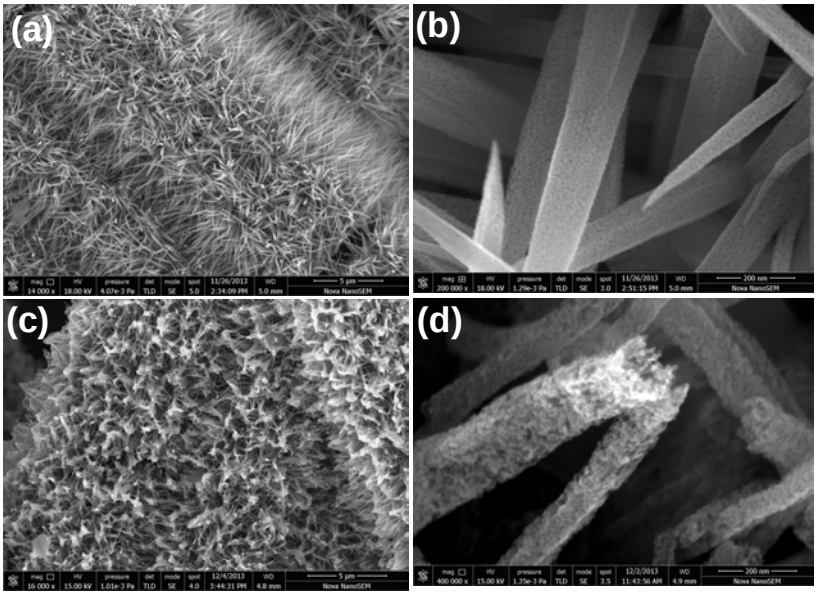

Figure 3 SEM images of the (a, b) NCO NWs; (c-d) NCS NWs.

observed. The large spaces between the interconnected carbon fibers assist in the faster transportation of ions to all electroactive surfaces. This reduces the diffusion limitation for high power supercapacitor applications. **Figure 3a** shows the uniformly grown one-dimensional NCO NWs on the surface of carbon fiber. The typical length of these nanowires ranges from 2-3 μm and width from about 10 nm (towards the tip) to 100 nm (towards the stem). Each nanowire.is separately and individually connected with the carbon fiber thereby facilitating the electronic and ionic transport to the whole active area. The High resolution SEM images (**Figure 3b**) show that the surface of the NCO NWs is quite smooth in nature. The images of the NCS NWs formed post-sulfurization shown in **Figure 3c-d** indicate no changes in their size and shape as compared to their NCO counterparts. This proves that the wet chemical sulfurization process does not lead to changes in the basic morphology of the nanowires. Interestingly though it is important to mention here that the sulfurization process gives

rise to enhanced surface roughness in the NCS morphology which can be clearly observed from **Figure 3d**. This roughness may be a result of the vigorous anion exchange reactions that take place between the oxides and sulfides at the surface of the NCO NWs during the wet chemical sulfurization process.

For understanding the micro-structural features of the nanowires in detail, High resolution transmission electron microscopy (HRTEM) imaging was performed on the samples. Porous NCO 1D nanostructure was found in the TEM image (**Figure 4a**). These polycrystalline nanowires are built by an assembly of smaller NCO nanoparticles (size ~10-15 nm). The lattice planes are identified with HRTEM images at higher magnification (**Figure 4b**). The inter lattice spacing was found to be ~ 0.28 nm, corresponding to the (220) plane. Energy Dispersive X-ray analysis (EDAX) (**Figure 5a)** reveals that the relative atomic ratios of the Ni, Co and O are close to 1: 2: 4 which is the stoichiometry of NCO, further confirming the presence and single phase character of this material. The copper and carbon peaks obtained in EDAX arise due to the TEM grid. TEM images of the NCS NWs are shown in **Figure 4c-d**, where it is clearly observed that there is no change in the morphology. The lattice spacing observed in the NCS NWs is 0.32 nm which corresponds to the 220 plane (**Figure 4d**) EDAX spectra of NCS with relative atomic ratios of the Ni, Co and S are close to 1: 2: 4 was shown in **Figure 5b.**

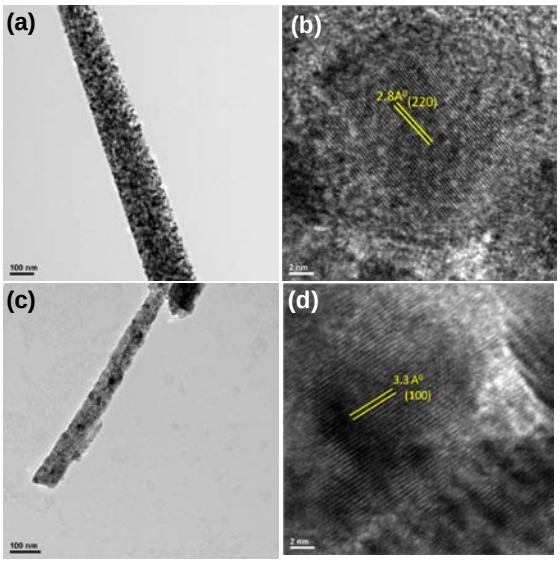

Figure 4 TEM images of the (a,b) NCO NWs; (c-d) NCS NWs

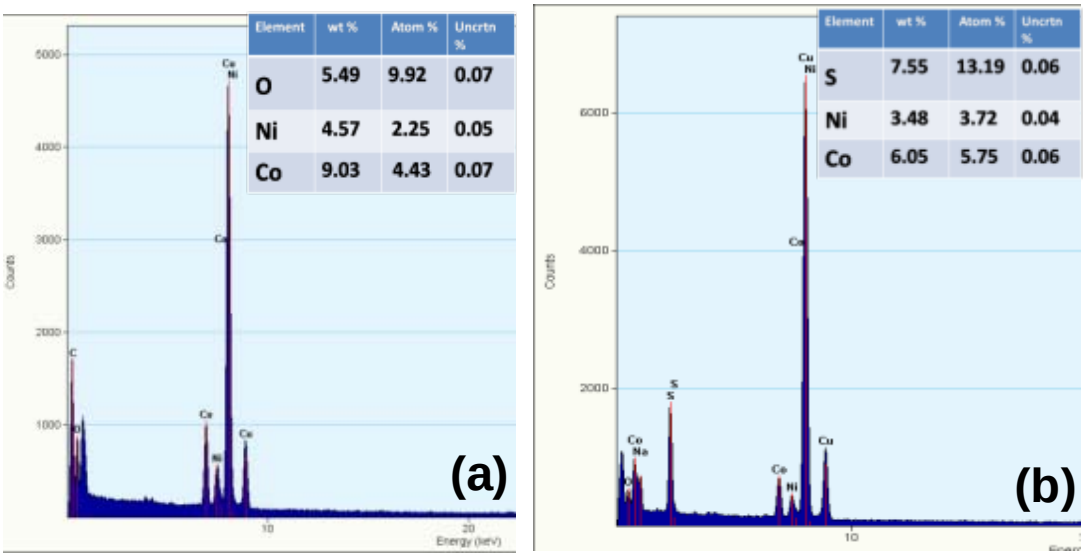

Figure 5 is EDAX spectra of (a) NCO and (b) NCS nanowires.

To investigate the electrochemical performance of the NCS NWs, we performed cyclic voltammetry (CV) measurements using a three electrode configuration (2M KOH electrolyte and a potential window ranging from 0-0.6 V). NCS on carbon fiber paper was used as the working electrode, Pt strip as the counter electrode, and Mercury/Mercury Oxide (Hg/HgO, 20% KOH) as the reference electrode. The CV curves obtained at different scan rates (1 mV/s - 8 mV/s) are presented in **Figure 6a**. The CV of NCS is different from the typical rectangular shape of double layer capacitance where adsorption and desorption of ions takes place at the interfaces of the electrode materials. From the CV curve obtained in our measurement, we can easily identify a pair of redox peaks (oxidation and reduction) which are highly reversible in nature. The large redox peaks indicate that the charge storage mechanism follows faradaic behavior and is pseudocapacitive in nature. The oxidation and reduction is brought about by the reaction of hydroxyl ions with both cobalt and nickel ions represented in the following equations:

$$NiS + OH^- \longrightarrow NiSOH + e^-$$

$$CoS + OH^- \longrightarrow CoSOH + e^-$$

With increasing scan rate, the oxidation peak is shifted towards the the positive potential and the reduction peak is shifted towards negative potential. This can be attributed to the electrolyte diffusion resistance. The CV curve of NCO shown in **Figure 7a** also

demonstrates a pseudocapacitive nature with reversible redox peaks like NCS corresponding to the oxidation and reduction of metal ions. The overall current (area under the curve) of the redox peaks in NCO is relatively less as compared to the NCS NWs for the same scan rate and identical electroactive surface area. From the CV curve at 5 mV/s, (**Figure 6b**) it can be clearly observed that the oxidation and reduction peak current of NCS NWs is around 6 times higher than that of NCO. This indicates an enhanced pseudocapacitive nature of NCS NWs in comparison to that of NCO.

As a control experiment, the bare carbon fiber paper electrode was also dipped in the electrolyte and CV measurement was carried out. An extremely low current was observed in the same (**Figure 7b**) indicating negligible capacitance contribution from

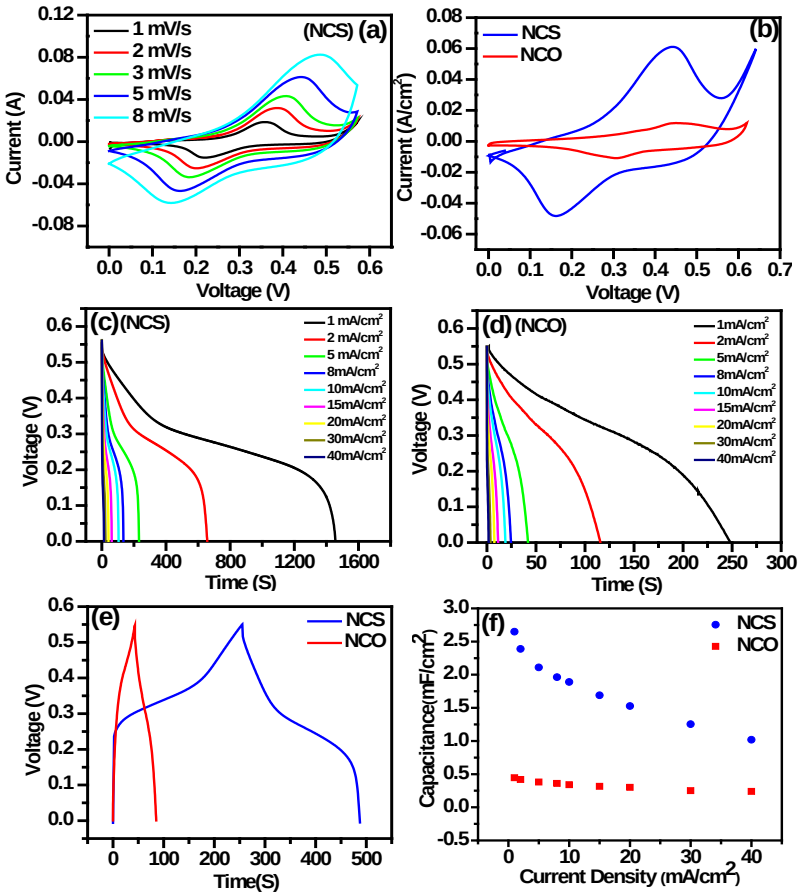

Figure 6 (a) Cyclic voltametry (CV) of the NCS NWs at different scan rates from 1 to 8 mV/s; (b) the CV plot of the NCO and NCS NWs at the scan rate of 5 mV/s; (c and d) are the charge discharge plots of the NCS and NCO, respectively, at different current density values from 1 to 40 mA/cm^2;(e) Charge-discharge plot of NCS and NCO NWs at the current density of 5 mA/cm^2; (f) the capacitance of the NCS and NCO NWs at different current densities.

the current collector. Galvanostatic charge-discharge measurement was also performed to determine the capacitance value as well as the rate capability of the NCS NWs. These experiments were performed in the current density range of 1-40 mA/cm^2 for both types of nanowires (NCO and NCS) (**Figure 6 c, d**). **Figure 6e** indicates the nature of the charge-discharge at 5 mA/cm2 for the NWs. The charge-discharge in both cases is extremely symmetric in nature with coloumbic efficiency of 97% confirming the highly reversible nature of the electrodes. It is important to notice that NCO NWs exhibit a strong potential drop from 0.3 to 0 volt whereas NCS shows a long plateau of charging and discharging within this potential range. This is because the integrated area of the CV curve for NCS within this potential range is higher than NCO. This result further indicates that substantially more faradaic reactions take place at the NCS surfaces as compared to the NCO case. The areal capacitance values were calculated from the charge-discharge curves by the equation

$$C_{arl} = \frac{I \cdot \Delta t}{\Delta V}$$

where C_{arl} is the areal capacitance (F/cm^2), 'I' is the current density (A/cm^2), ΔV is the potential window and Δt is the discharge time. The specific capacitance values for different current densities are plotted in **Figure 6f**. The NCS NWs array shows a maximum capacitance of 2.65 F/cm^2 at a current density of 1 mA/cm^2 which is almost 6 times higher as that of pristine NCO NWs. The NCS NWs deliver higher areal capacitance as compared to NCO within the current density range of 1- 40 mA/cm^2. This kind of enhancement has been previously observed in the case of Co_3O_4 and Co_9S_8, where the charge storage performance increases after the sulfurization process.[21] After increasing the current density by 40 times, the capacitance retention of the NCS NWs is observed to be around 40%. This capacitance retention is better or comparable to other sulfide based materials reported recently eg. 78% capacitance degradation (22% retention) taking place in CoS_2 ellipsoids on increasing the current density from 0.5 A/g to 10 A/g, 15 and 60% capacity degradation taking place in NiS hollow nanospheres after increasing the current density from 4 to 10.2 A g^{-1}.[14]

The gravimetric capacitances were also calculated for the NCO and NCS NWs at the current density of 5 mA/cm^2. NCO NWs show a specific capacitance of 413 F/g whereas the NCS NWs show a much higher specific capacitance of 2027 F/g. It is important to notice that even though the surface area of the NCS sample (31 m^2/g) is much less than

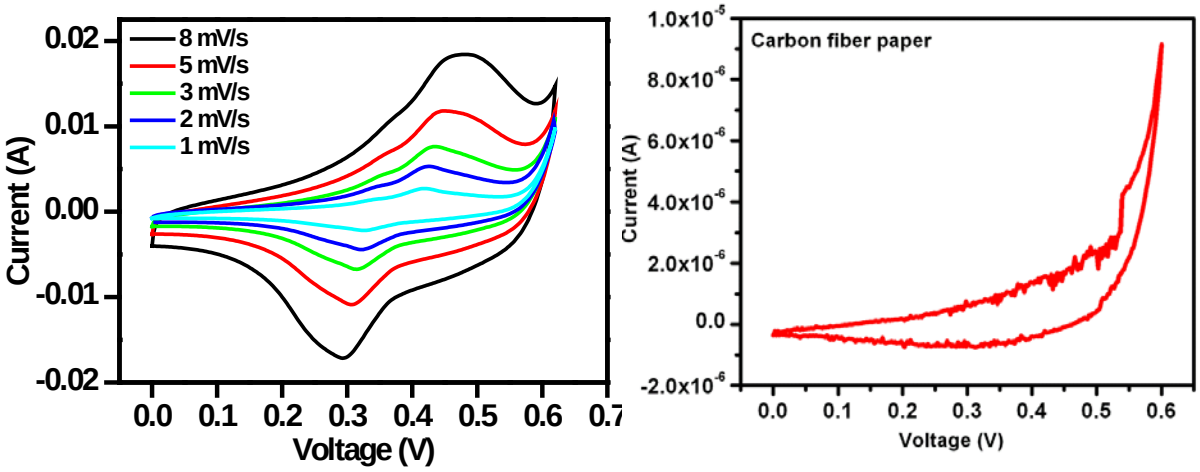

Figure 7 (a) is the Cyclic voltametry of the NCO NWs in 2(M) KOH (b) is the Cyclic voltametry of the carbon fiber paper in 2(M) KOH

that of NCO sample (89 m^2/g) (**Figure 8**), the capacitance value of NCS is significantly higher than that of NCO. We can thus conclude that the higher capacitance of NCS results mainly because of the increase in the conductivity of NCS NWs after sulfurization of NCO NWs. The high conductivity of the NCS NW helps reduce the cell resistance facilitating the electron transfer which can yield an increase in the capacitance value. Even with a lower surface area of 20 m^2/g Chen et al. achieved a capacitance value of 1149 F/g for powder sample of $NiCo_2S_4$ urchin nanostructures. Powder sample has the problem of diffusion of electrolyte inside into the bulk of the

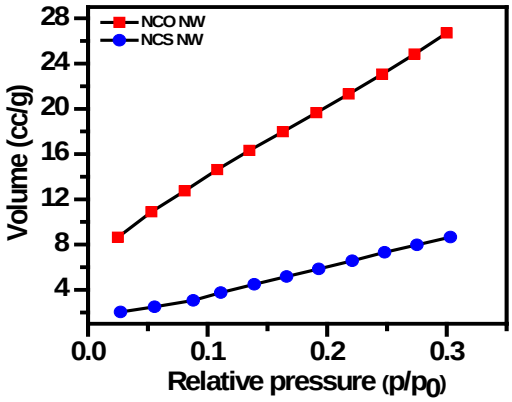

Figure 8 is the BET surface area of the of the NCO and NCS nanowires upto p/po 0.3.

electrode. In our case the surface area is higher and the nanostructure is not only oriented but is directly anchored on a conducting substrate which renders a robust electrical contact. Therefore, in addition to a superior overall access of the nanostructure surface to the electrolyte (ions), the electrical conductivity is also high, which results in increase in the capacitance value.

The high rate performance is mainly because of the hierarchical nanostructure which assists in the quick and facile interaction of the electrolyte ions with the redox surfaces in order to make the faradaic process feasible. It reduces the electrolyte diffusion time to the surfaces resulting in good electrochemical performance even at a very high current density. The capacitance values clearly reveal the advantage of any single component based electrode material for supercapacitor applications.

We now compare the electrochemical performance of our material with recent reports in the literature. Huang et al. have reported a capacitance of 2.07 F/ cm^2 at a current density of 10 mA/cm^2 for hybrid NCO@Ni-Co hydroxide nanostructures.[20] Yu and coworkers synthesized NCO@MnO_2 on nickel foam by two step process and obtained a capacitance 2 F/cm^2 at a current density of 10 mA/cm^2.[22] Other hybrid nanostructures have also been explored in this context. These include MnO_2@NiO NWs array (0.35 F cm^{-2} at 9.5 mA cm^{-2}) [23], NiO@TiO_2 nanotube arrays (3F cm^{-2} at 0.4 mA cm^{-2}) [24], Co_3O_4 NW@MnO_2 nanosheet core-shell arrays (0.56 F cm^{-2} at 11.25 mA cm^{-2}) [25] etc. (These details are also summarized in the in the **Table** below).

Our work demonstrates that a ternary sulfide based single component nanostructure exhibits an excellent performance comparable to hybrid nanostructures reported in the literature which is technologically important. The option of making hybrid materials using NCS can be explored in the future. The gravimetric capacitance of the NCS NWs is also considerably higher than the recent reported urchin-like nanostructures of NCS by Chen et al. [18] (1149 F/g at the current density of 1 A/g) and NCS sheets on graphene substrate (1451 F/g at the current density 3A/g) by Peng et al.[27]

Table

Materials	Areal capacitance (F/cm^2)	Current Density (mA/cm^2)
Single crystal nanoneedle arrays [26]	**1.01**	**5.06**
NiO-TiO_2 nanotube arrays [24]	**~3**	**0.4**
Co_3O_4@MnO_2 hybrid nanowires [25]	**0.56**	**11.25**
$Ni(OH)_2$/USY[28]	**0.86**	**10**
$NiCo_2O_4$@NiCo -hydroxides [20]	**2.17**	**10**
$NiCo_2O_4$@MnO_2 hybrid nanowire[22]	**2.06**	**10**
Co_9S_8 nanorod [21]	**0.86**	**10**
$NiCo_2S_4$ nanowires (This work)	**1.89**	**10**

As supercapacitors are the best source of power for portable devices, low resistance of the electrode materials is electrochemically preferred for better applicability. To further study the superiority of NCS over NCO, electrochemical impedance spectroscopy (EIS) was performed at the bias potential of 0.2 V over the frequency range of 0.01Hz-10^5 Hz. The impedance spectrum can be divided into two parts: a high frequency region characterized by the presence of a semicircle and the low frequency region characterized by a straight line. High frequency region is particularly important as it can be used to characterize the material properties like equivalent series resistance (sum of contact resistance, electrolyte resistance, and material resistance) from the intercept of the semicircle on the real axis. The charge transfer resistance, R_{ct}, can be obtained from the diameter of the semicircle.

Figure 9a-b shows the Nyquist plots for NCO and NCS. The real axis intercept in the case of NCO and NCS is 5.80Ω and 1.65Ω, respectively, which clearly shows the high conductivity of NCS over NCO. This is reflected in the higher capacitance with NCS.

Further the smaller semicircle in the case of NCS clearly indicates very low charge transfer resistance (R_{ct} ≈ 0.16Ω) over that of NCO (R_{ct} ≈ 1.09Ω). In the mid-frequency

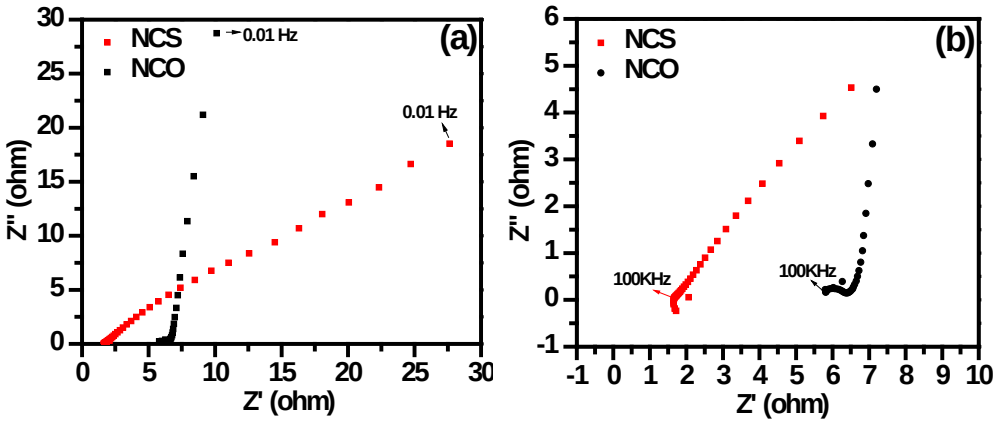

Figure 9 (a) Electrochemical impedance spectra of the NCO and NCS NWS; (b) magnified impedance spectra over the higher frequency region.

range a straight line projected at 450 is observed in the NCS case showing diffusion of ions into the electrode material reflecting the high porosity and well-developed pore architecture, while in the case of NCO over the same frequency region a straight line parallel to imaginary axis is observed, showing ideal EDLC behavior without diffusional effects.

To evaluate the stability and durability of the synthesized NCS NWs, cyclic stability of the material was also tested up to 1000 cycles at a very high current density of 20 mA/cm^2 (**Figure 10a**). The electrode shows very long term stability even at such high current density. 73% of the capacitance is retained after 1000 cycles. This degradation of capacitance value is common for metal sulfides.14,15,28 Cyclic voltametry and charge discharge studies were also performed for NCS NWs after 1000 cycles (inset **Figure 10b-c**) where the observed decrease in the overall current in CV measurement corresponds to lower discharge time. Lowering of the capacitance value may be attributed to the removal of the active materials (NCS) gradually with cycling.

Further, comparison of Nyquist plots (**Figure 10d**) for NCS sample just after the first cycle and after 1000th cycle shows that the projected Warburg diffusion decreases at higher frequencies in the initial cycles compared to the measurements after 1000

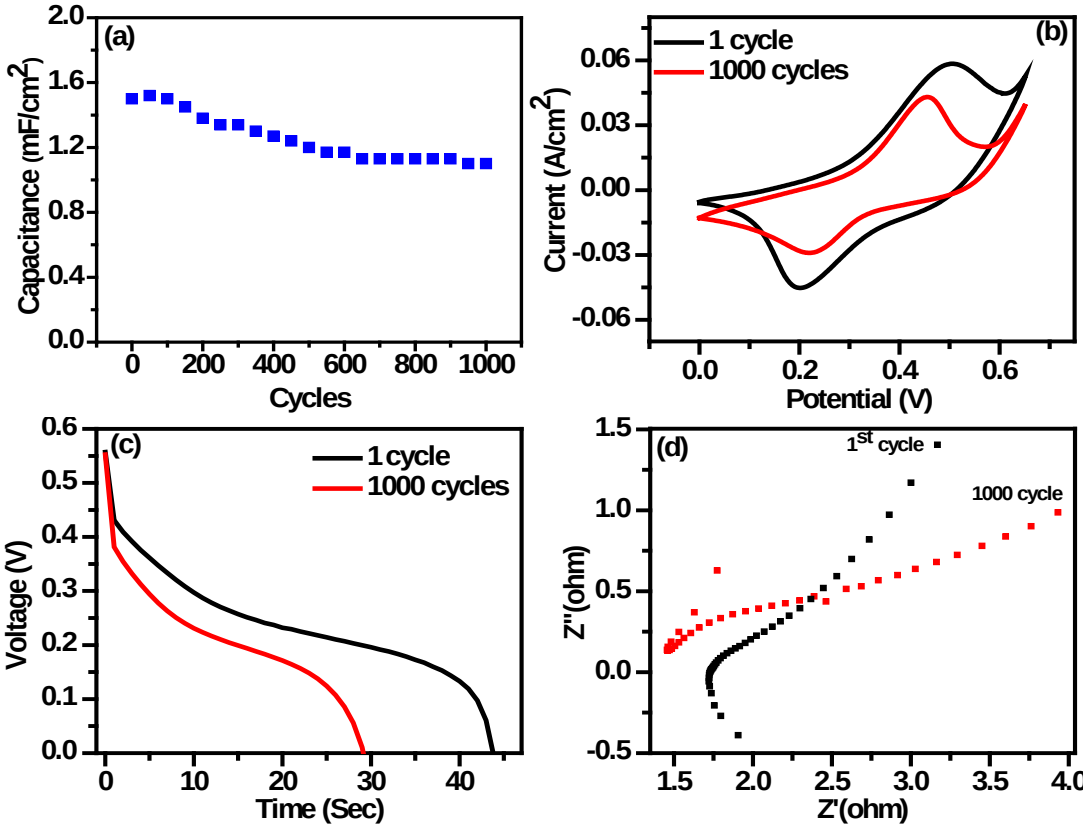

Figure 10(a). Electrochemical cyclic stability of the NCS NWS upto 1000 cycles at current density of 20 mA/cm2, (b) Cyclic voltammetry study of NCS NWs at 1st cycles and 1000 cycle (c) Discharge profile of NCS NWs at 1st cycles and 1000 cycle (d) electrochemical impedance spectrum of 1st and 1000 cycle of NCS NWs.

cycles. The longer length of projected Warburg line in the initial cycles points to the lesser diffusion resistance initially and with cycling the resistance increases due to degradation of material as explained earlier in the cycling stability plot of NCS. Overall, the carbon fiber paper supported NCS NWs show sufficient cyclic stability at a very high current density, which is important for practical applications.

2.8 Conclusion

We have demonstrated the synthesis and direct growth of one-dimensional NCS NWs array on carbon fiber paper by a simple wet chemical closed sulfurization process on hydrothermally grown NCO NWs at 120ºC. The charge storage behavior of both, the NCS and NCO NWs, is studied in an aqueous electrolyte. It is observed that the NCS NWs exhibit much better electrochemical charge storage performance than the NCO counterparts in a process that does not involve the use of insulating binders and conducting carbon. The better performance of the NCS NWs is attributed to an increase in the electrical conductivity and surface roughness; properties which assist in faster redox reactions through better electron transport.

The carbon fiber paper supported NCS NWs display a very high rate capability and cyclability which can be attributed to their morphology that assists in ion diffusion and a complete utilization of the surface of the nanostructures. Furthermore these structures can be further engineered into hybrid core shell 3D nanostructures with different metal oxides and sulfides to improve the areal capacitance to even higher values.

2.9 References

[1] Simon, P.; Gogotsi, Y. Nature Materials, **2008**, 7.

[2] Dunn, B.; Kamath, H.; Tarascon, J. Science, **2011**, 334, 92.

[3] Zhoua, Z.; Benbouzida, M.; Charpentierb, J. F.; Scuillerb, F.; Tang, T. Renewable and Sustainable Energy Reviews, **2013**, 18, 390.

[4] Zhang, L. L.; Zhao, X. S. Chem. Soc. Rev., **2009** , 38, 2520.

[5] Yadav, P.; Banerjee A.; Unni, S.; Jog J.; Kurungot, S.; Ogale, S. Chem.Sus.Chem., **2012**, 5, 2159.

[6] Zhu, Y.; Murali, S.; Stoller, M. D.; Ganesh,K. J.; Cai,W.; Ferreira, P. J.; Pirkle,A.; Wallace, R. M.; Cychosz, K. A.; Thommes,M.; Su,D.; Stach, E. A.; Ruoff, R. S. Science, **2011**, 332.

[7] Hahm, M. G.; Leela, A.; Reddy, M.; Cole, D. P.; Rivera, M.; Vento, J. A.; Nam,J.; Jung, H. Y.; Kim, Y. L.; Narayanan, N. T.; Hashim, D.; Galande, P. C.; Jung, Y. J.; Bundy, M.; Karna, S.; Ajayan, P. M.; Vajtai, R. Nano Lett., **2012**, 12, 5616.

[8] Hu, C-C.; Chang, K-H.; Lin, M-C.; Wu, Y-T. Nano Lett., **2006**, 6, 2690.

[9] Zhang, G.; Lou, X. W. (D.). Scientific Reports., **2013**, 3, 1470.

[10] Yang, L.; Cheng, S.; Ding, Y.; Zhu, X.; Wang, Z. L.; Liu, M. Nano Lett., **2012**, 12, 321.

[11] Xia, X-h.; Tu, J-p.; Mai, Y-j.; Wang, X.-l.; Gu, C-d.; Zhao, X-b. J. Mater. Chem., **2011**, 21, 9319–9325.

[12] Zhong, J-H.; Wang,A-L.; Li, G-R.; Wang, J-W.; Ou, Y-N.; Tong, Y-X. J. Mater. Chem., **2012**, 22, 5656.

[13] Zhu, T.; Chen, J. S.; Lou, X. W. J. Mater. Chem., **2010**, 20, 7015.

[14] Zhu, T.; Wang, Z.; Ding, S.; Chen, J.S.; Lou, X. W. (D.) RSC Adv., **2011**, 1, 397.

[15] Zhang, L.; Wu, H. B.; Lou, X. W. (D.) Chem. Commun., **2012** ,48, 6912

[16] Wei,T-Y.; C-H. Chen,; Chien, H-C.; Lu, S-Y.; Hu, C-C. Adv. Mater., **2010**, 22, 347

[17] Zhang ,G.; Lou, X. W. (D.) Adv. Mater., **2013**, 25, 976

[18] Chen, H.; Jiang, J.; Zhang, L.; Wan, H. Qi, T.; Xia, D. DOI: 10.1039/b000000x

[19] Rakhi, R. B.; Chen, W.; Cha, D.; Alshareef, H. N. Nano Lett., **2012**, 12, 2559

[20] Huang, L.; Chen, D.; Ding,Y.; Feng, S.; Wang, Z. L.; Liu, M. Nano Lett., **2013**, 13, 3135.

[21] Xu, J.; Wang, Q.; Wang,X.; Xiang, Q.; Liang, B.; Chen, D.; Shen,G. Acs Nano., **2013,** 7, 5453.

[22] Yu, L.; Zhang,G.; Yuan C.; Lou, X. W. (D.) Chem. Commun., **2013**,49, 137

[23] Liu, J.; Jiang, J.; Bosmanc, M.; Fan, H. J. J. Mater. Chem., **2012**, 22, 2419

[24] Kim, J-H.; Zhu, K.; Yan, Y.; Perkins, C. L.; Frank, Arthur J. Nano Lett., **2010**,10, 4099

[25] Liu, J.; Jiang , J.; Cheng ,C.i; Li , H.; Zhang, J.; Gong, H.; Fan, H. J. Adv. Mater., **2011**, 23, 2076

[26] Zhang, G. Q.; Wu, H. B.; Hoster,H. E.; Chan-Parkb, M. B.; Lou, X. W. (D.) Energy Environ. Sc., **2012**, 5, 9453

[27] Peng, S.; Li, L.; Li, C.o.; Tan, H.; Cai, R.; Yu, H.; Mhaisalkar, S.; Srinivasan, M.; Ramakrishna ,S.; Yan,Q. Chem. Commun., **2013**,49, 10178.

[28] Xinga, Z.; Chua, Q.; Rena, X.; Tiana, J.; Asirib, A. M.; Alamryb, K. A.; Al-Youbib A. O.; Sun, X. Electrochemistry Communications, **2013**, 32 , 9.

Chapter-3

3.1 Title

Crumpled-sheet-assembled perforated carbon cuboids by MOF pyrolysis: A highly effective cathode active material for ultra-high energy density Li-ion hybrid electrochemical capacitors (Li-HEC)

3.2 Abstract

Lithium ion hybrid capacitors (Li-HEC) have attracted significant attention for next generation advanced energy storage technologies to satisfy the demand of both high power density as well as energy density. Herein we report the very high surface area 3D cuboids carbon synthesized from metal organic framework (MOF) as a cathode material with $Li_4Ti_5O_{12}$ as anode for high performance Li-HEC. The energy density of the cell is ~65Wh kg^{-1} which is significantly higher than the commercially available activated carbon (~36Wh kg^{-1}) and symmetric performance of the MOF derived carbon (MOF-DC, ~20Wh kg^{-1}). The MOF-DC/$Li_4Ti_5O_{12}$ Li-HEC assembly also showing good cyclic performance with ~82% of initial value (~25Wh kg^{-1}) after 10000 galvanostatic cycles under high rate cyclic condition. This results clearly indicates that MOF-DC is very promising candidates in future for drive P-HEV in Li-HEC configuration.

3.3 Introduction

Of late, metal organic frameworks (MOF) have become one of most promising architectures in material science by virtue of their unique forms and properties. Basically, MOF is a crystalline assembly of metals and ligands, where the ligands are coordinated with metal ions to form a highly open 3D framework. Facile synthesis procedures and intrinsic porosity make MOFs attractive candidates for a wide range of

applications includes catalysis, sensors, drug delivery, gas adsorption, gas separation etc. [1-6]

Indeed MOFs are also very promising precursors in the context of synthesis of a variety of functional inorganic and carbon-based materials for different applications. Porous Fe_2O_3, ZnO, CuO and other oxide nanostructures synthesized using MOFs have been evaluated for diverse applications such as water purification, removal of organic pollutants, glucose detection, supercapacitor, oil recovery etc.[7-9] Some of these oxides have also been examined as anodes for Li-ion battery (LIB) applications with promising results.[10-12] High surface area carbons derived from MOFs have been effectively used for CO_2 uptake and hydrogen adsorption applications.[13,14] Nitrogen rich carbons from nitrogen-containing ligand-based MOFs have also been synthesized and successfully used for electro-catalysis in oxygen reduction reaction. [15] MOF-derived carbons have been examined for charge storage applications as well, especially supercapacitors, in both aqueous (H_2SO_4 and KOH) and organic (ionic liquid) electrolytes.

Chaikittisilp et al.[16] directly pyrolyzed the Zn-based zeolitic imidazolate framework (ZIF-8) at different temperatures to realize a high BET surface area of 1110 m^2g^{-1} and an impressive specific capacitance value of 214 F g^{-1} at a scan rate of 5mVs^{-1} in aqueous H_2SO_4 medium. Akita and co-workers [17] used the 3D channels of the MOF-5 as a template for polymerized poly-furfuryl alcohol, which upon pyrolysis at 1000°C for 8 h under Ar flow yielded nano-porous carbon with a high surface area of 2872 m^2g^{-1}. A specific capacitance of 233 Fg^{-1} (@ 2 mV s^{-1}) and 312Fg^{-1}(@1 mV s^{-1}) was obtained in 1.0 (M) H_2SO_4. Hu et al.[18] successfully synthesized different forms of carbon using MOF-5 as a template for loading phenolic resin or ethylenediamine and carbon tetrachloride as carbon source(s). The porous carbon obtained by pyrolyzing the template loaded MOF-5 was activated using KOH to tune the porosity and surface area. Out of the two routes followed, the carbon tetrachloride and ethylenediamine loaded MOF-5 showed the higher surface area (2222 m^2g^{-1}). They obtained a maximum capacitance of 271Fg^{-1} (energy density = 9.4 Whkg^{-1}) in aqueous medium and 156Fg^{-1} (energy density=31.2 Whkg^{-1}) in organic medium (tetraethyl-ammonium-tetrafluoro-borate).[18] Yuan et al.[19] also used Zn-based metal-organic coordination polymer as a

template and glycerol as a carbon precursor to synthesize worm-like mesoporous carbon. It showed high specific surface area (2587 m^2g^{-1}) and a large pore volume (3.14 cm^3g^{-1}). They obtained a specific capacitance of 344 Fg^{-1} at the current density 0.5 A g^{-1}, in aqueous KOH electrolyte . In most such studies on supercapacitor, charge storage employing MOF-derived carbonaceous materials experiments have been predominantly performed in symmetric configurations, thereby limiting the energy density to low values (typically 9-30 $Whkg^{-1}$). These values are significantly lower than those desired for zero-emission transportation applications such as electric vehicles (EV, min 150 Wh kg^{-1}) and plug-in hybrid electric vehicles (P-HEV, 57 to 97 Wh kg^{-1}).[20]

In order to improve the energy density of supercapacitors (without significantly compromising on power density), Amatucci et al .[21] first introduced the concept of integrating two well-known electrochemical energy storage device platforms, namely LIB and supercapacitors. Generally, these so-called Li-ion hybrid electrochemical capacitors (Li-HEC) are fabricated with high surface area carbonaceous materials along with Li-intercalating material as counter electrode. [21-26] The high surface area carbon and insertion type electrode provide the high power capability and high energy density capability, respectively. Thus, higher power density than LIB and higher energy density than a supercapacitor are achievable in Li-HEC. Several research efforts have been undertaken to realize a good insertion anode for such a device and spinel phase $Li_4Ti_5O_{12}$ has been found to be appealing over others in terms of its favorable electrochemical characteristics.[27-36] Unfortunately, however, only limited work has appeared in the literature thus far on the development of specially engineered carbonaceous electrodes for desirable property features for this Li-HEC application.

Herein, we present the first report on the interesting case of MOF-derived high surface area porous carbon as cathode active material for Li-HEC applications, along with $Li_4Ti_5O_{12}$ as counter electrode in an organic medium. My contribution in this work is mainly on synthesis and characterization of carbon derived from MOF-5.For comparison, MOF derived symmetric supercapacitor is also fabricated and tested in the same organic medium. We have specifically chosen (reasons discussed further in the

text) the zinc based MOF (MOF-5) as a precursor to yield the high surface area porous carbon (MOF derived carbon, or MOF-DC). Extensive powder and electrochemical studies have been conducted for both configurations stated above and are described in detail.

3.4 Experimental Section

Zinc nitrate hexahydrate ($Zn(NO_3)_2.6H_2O$), benzene 1,4 di-carboxylic acid (BDC) and di-methyl formamide (DMF) were used for the synthesis of MOF-5. In a typical synthesis process, 10.4 g of $Zn(NO_3)_2.6H_2O$ and 2 g of BDC were simultaneously dissolved into 140 ml. of DMF. After complete dissolution, the mixture was transferred into a round bottle flask with a condenser and heated at 120^oC for 24 h. After cooling, Zn-MOF was collected from the flask and washed with DMF several times. Thereafter, the Zn-MOF was immersed into dry chloroform for two days, with the chloroform replaced thrice daily. Finally, the MOF-5 crystals were harvested and heated under vacuum at 140^oC overnight. Porous carbon was obtained by pyrolysing the above MOF-5 at 1000 ^oC for 8 h under Ar flow. The heating rate was 5 ^oC per minute.

3.5 Results and discussion

For the synthesis of high surface area porous carbon, MOF-5 ($Zn_4O(OOCC_6H_4COO)_3$) was chosen as the precursor, since it is one of the attractive MOFs which exits in a three dimensional framework with cavity diameter of 1.8nm.[37] The fact that it has Zn is also very important from the standpoint of getting the desired porous carbon as discussed next.

During the MOF carbonization process in flowing Argon, as the temperature is increased the decomposition of solvent molecules (50-200^oC) and breakdown of MOF host (400-500^oC) result in the formation of carbonaceous materials along with ZnO at a relatively lower temperature (**Figure 1**). When the temperature rises above 800^oC carbo-thermal reduction of ZnO occurs and subsequently Zn metal is formed

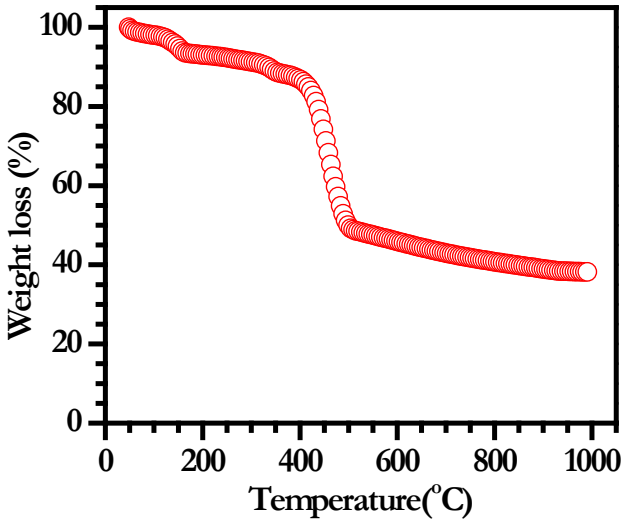

Figure 1 Thermo-gravimetric curves for MOF-5 in Ar flow at 5 ^{o}C min^{-1}

(ZnO + C→ Zn + CO↑). Zn being a low boiling point element, it gets evaporated to form a high surface area porous carbon above 907^{o}C with excellent porosity. It is well established that Zn based salts (ex.$ZnCl_2$) provide beneficial effects (the so-called activation) during the synthesis of high surface area porous carbons with tailored meso-/micro-porosity.

Figure 2a shows the X-ray diffraction (XRD) pattern of MOF-5 exhibiting fairly intense reflections. All the observed reflections are consistent with the literature and confirm the high purity of the synthesized MOF-5 phase.[38] The XRD pattern of the MOF derived carbon (MOF-DC) material obtained after pyrolysis of MOF-5 at 1000^{o}C under flowing argon. (**Figure 2b**) is rather featureless and shows two broad humps near 2θ of 240 and 430. The locations and peak widths of these humps imply the formation of almost amorphous or nanocrystalline carbon. Indeed the lower peak at about 2θ of 240 is downshifted from the pure graphite location of about 260 indicates more of a turbostratically disorder represented by nanoscale graphene-like units assembled in a topologically disordered fashion. This is also borne out by Raman spectra, discussed next. Further, zinc oxide or metallic impurity related reflections are not seen which confirms the complete removal of such secondary phases during the high temperature carbonization and is consistent with the thermo-gravimetric analysis (**Figure 1**).

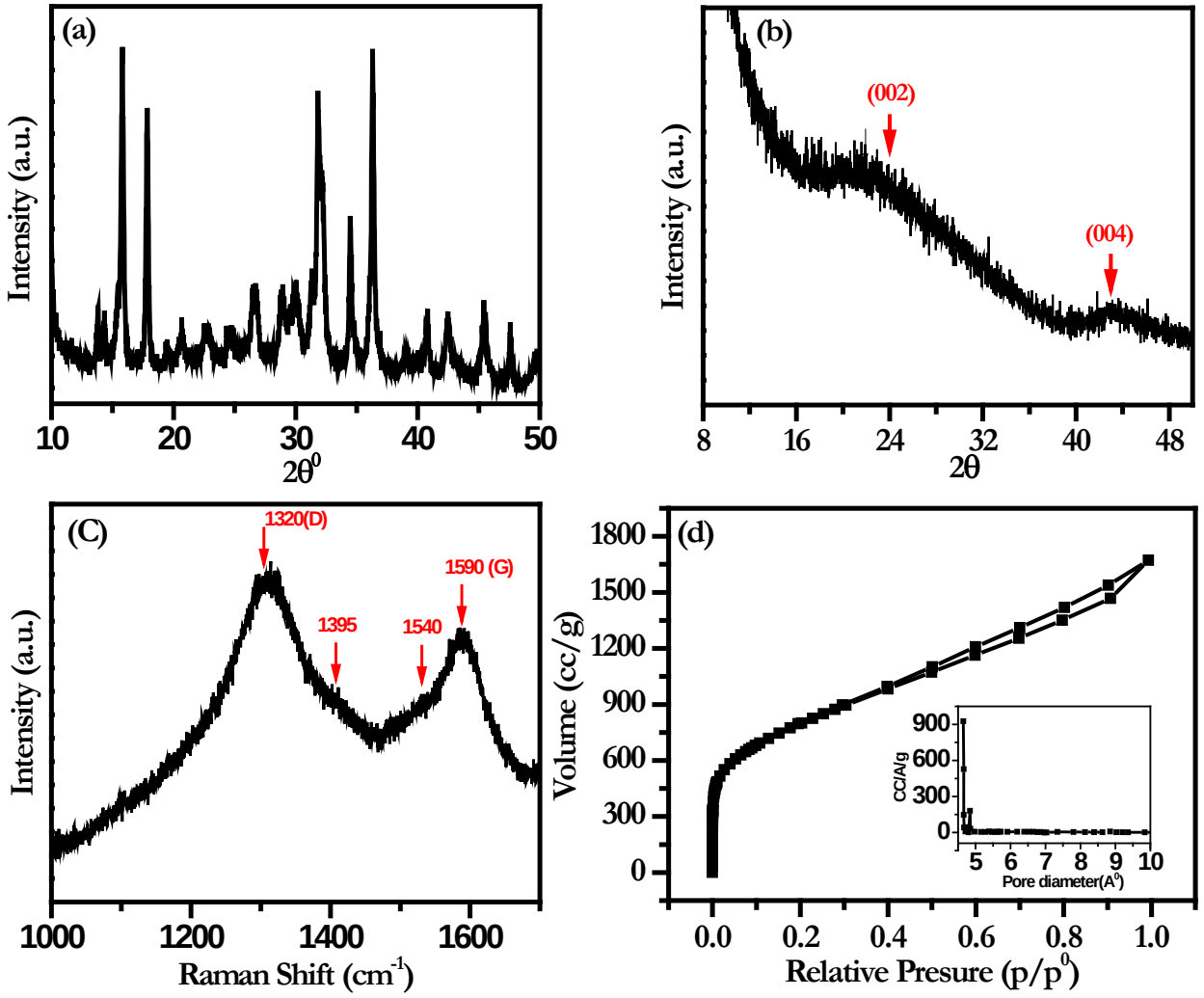

Figure 2 Powder X-ray diffraction pattern of (a) MOF-5, and (b) MOF-5 pyrolyzed at 1000°C under Ar flow, (MOF-DC); (c) Raman spectrum of MOF-DC, and (d) N2 adsorption/de-sorption isotherms of MOF-DC, Inset: Pore size distribution

To study the nature of the carbon formed during the carbonization process more precisely, Raman spectrum was recorded and the same is shown in **Figure 2c**. The Raman spectrum of MOF-DC shows well-defined characteristic bands at ~1320 and ~1590 cm^{-1} which belong to the D and G modes of the carbon, respectively. The D band is identified as the defect band because of the k-point phonon mode of A_1g symmetry and G band is associated with E_2g mode of sp^2 type carbon. [39-41] The intensity ratio between D and G bands(I_D/I_G) provides useful information about the degree of crystallinity of the carbonaceous material.[29, 39] In the present case, the ratio is calculated to be 1.17, which clearly shows the disordered nature of MOF-DC. Further the emergence of two humps at around ~1385cm^{-1} and ~1540cm^{-1}can be clearly seen

in the Raman plot. The ~1540cm^{-1} peak can be assigned to a significant amount of different form of sp^2 content other than graphitic sp^2 carbon which may be present for turbostratically disordered carbons.[42] The peak at ~1385cm^{-1} has been observed in the various nitrogen and boron doped graphitic carbons. Its presence could also be attributed to defects induced in the carbon lattice by its folding or defects created by presence of the non-graphitic sp^2 content. The XRD and Raman data together suggest that this carbon is mostly of turbostratic character wherein very limited local nanoscale graphitization occurs due to low heating temperature, and such local units get stacked up in a topologically disordered fashion.

BET surface area measurements were also carried out and the nitrogen adsorption/de-sorption isotherms are presented in **Figure 2d** along with the pore size distribution. A steep increase in gas adsorption at relatively low pressure indicates the presence of high concentration of micropores in MOF-DC. Additionally, the slope is also noted under further increase of the relative pressure which confirms the existence of mesoporosity. The hysteresis curve at the time of desorption also parallels the presence of mesoporosity in MOF-DC. The BET specific surface area of the sample is 2714 m^2 g^{-1}. This value is almost close with the theoretical surface area of a well separated graphene layer. This is seen to have been realized in our case because of the presence of a high concentration of micropores. Such pore formation takes place because of the self-activation of Zn metal and its subsequent evaporation during the final carbonization process. The Pore-size distribution of MOF-DC is shown in **Figure 2d** (inset) which anchors predominately near~0.5 nm, which confirms the existence of microporosity.

Morphological and micro-structural investigations of MOF-DC were also carried out by FE-SEM and HR-TEM. The FE-SEM data are shown in **Figure 3a-c**. From **Figure 3a** it can be seen that a cuboid type of carbon morphology evolves in the pyrolysis process. Each cuboid (**Figure 3b**) is seen to have been assembled from crumpled graphene-like sheets. Moreover, a significant density of micro and mesopores can be clearly noticed (**Figure 3c**). The concurrent presence of crumpled sheet type morphology and mesoporosity together with abundant micropores are very important factors from the

standpoint of the adsorption area accessibility. If the sheets were not crumpled the stacking issue degrades the area accessibility dramatically.

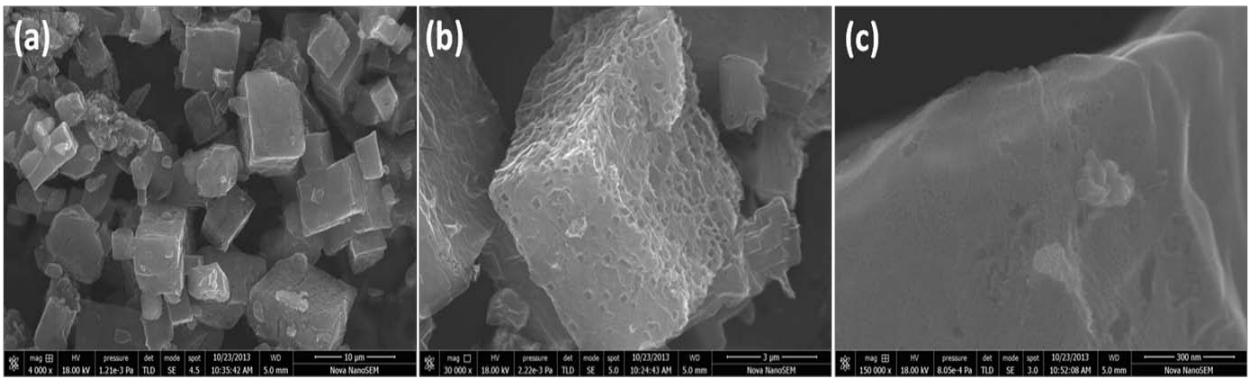

Figure 3 (a-c) FE-SEM images of MOF-DC at different magnifications

HR-TEM images (**Figures 4a-f**) bring out a very interesting form of self-similar hierarchical assembly of ultrathin (highly transparent to TEM electrons) sheets. **Figures 4a and 4b** show peculiar cellular porous morphology showing projections of cuboid type form at various length scales. **Figure 4c** makes this amply clear where about 20 nm type cells are seen to assemble into 200 nm cells which then form the overall cuboid

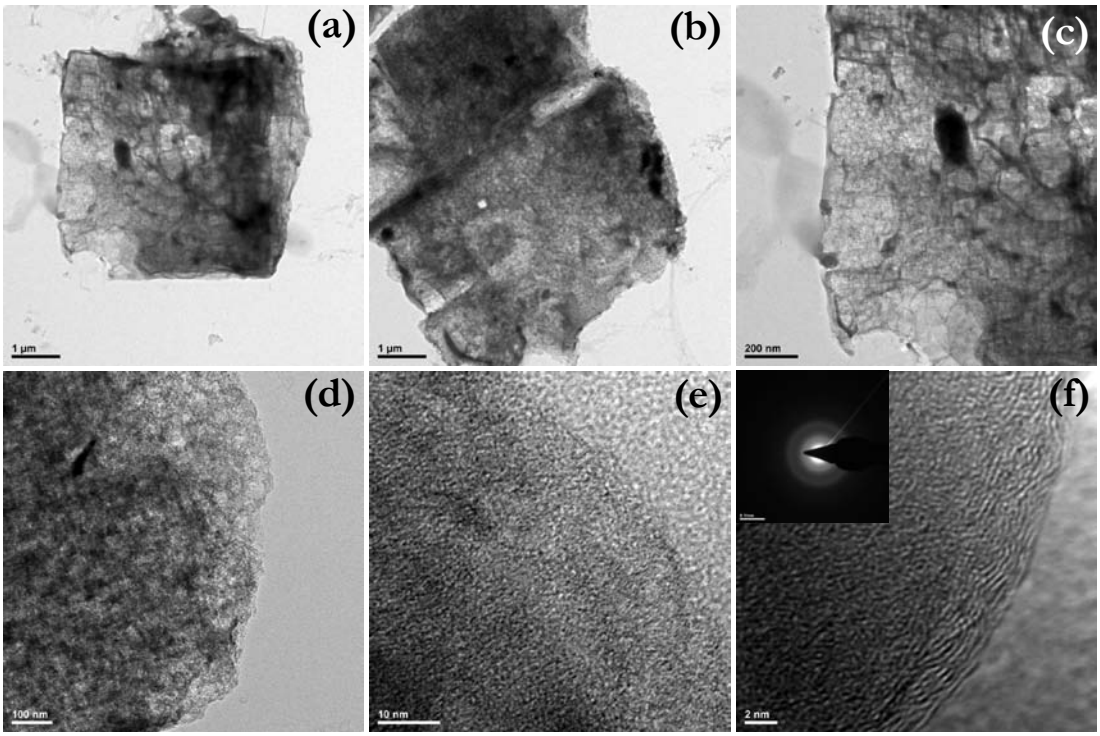

Figure 4(a-f) HR-TEM images of MOF-DC at different magnifications. The SAED pattern is given in the inset of (f).

which is several microns in size. **Figure 4d** reveals the nm scale details of the tiny cells, while **Figure 4e** brings out the ultrathin layered character of the sheet assembly. **Figure 4f** shows the nature of internal disorder which is consistent with the broad XRD peaks and Raman signatures. Single electrode performance of MOF-DC is very crucial to adjust the mass loading between the counter electrodes ($Li_4Ti_5O_{12}$) and eventually to attain high energy density Li-HEC configuration. In the case of a symmetric supercapacitor configuration (fabricated with the same mass loading), the applied potential is divided between the two electrodes which is mainly because both electrodes undergo the same charge storage mechanism.[43] On the other hand, high surface area carbonaceous cathode involves the double layer formation and $Li_4Ti_5O_{12}$ undergoes Li-insertion/extraction reaction in the Li-HEC assembly.[21, 22, 25] Thus, the applied potential will be divided according to the specific capacitance of the respective electrodes. Therefore the mass balance between the two electrodes is very important for the Li-HEC assembly.

Single electrode performance of MOF-DC was evaluated with respect to metallic lithium (Li/MOF-DC) and the typical electrochemical profiles are as illustrated in **Figure 5**. **Figure 5a** represents the typical galvanostatic charge-discharge curves for the MOF-DC

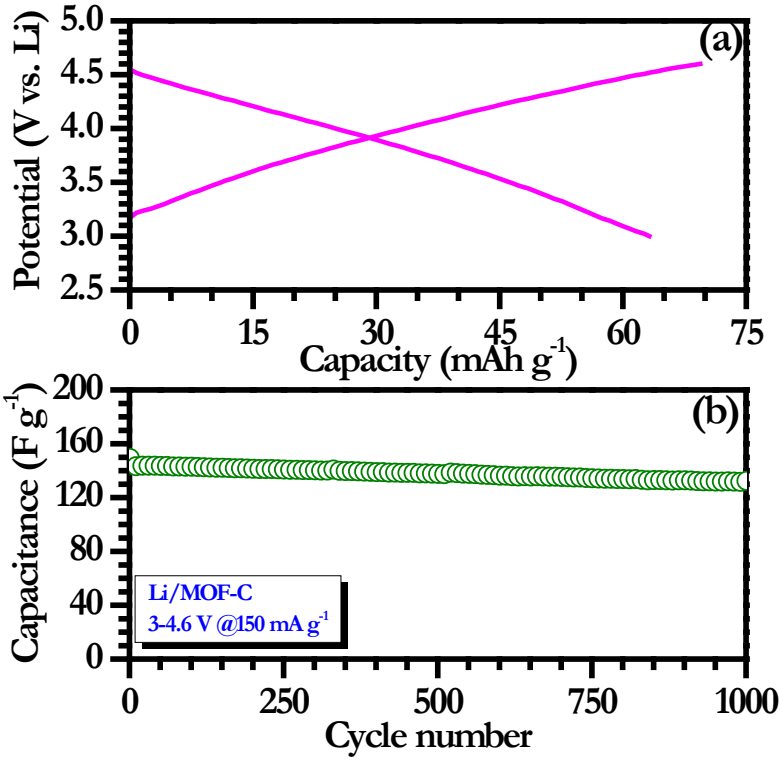

Figure 5 (a) Typical galvanostatic charge-discharge curves of MOF-DC in single electrode configuration (half-cell) tested between 3-4.6 V *vs.* Li, in which metallic lithium acts as both counter and reference electrode, and (b) Plot of specific discharge capacitance *vs.* cycle number.

sample cycled between 3-4.6 V vs. Li under ambient conditions. A linear increase with time (i.e. capacity) with respect to the potential is noted which indicates perfect electric double layer formation (anion double layer) across the electrode/electrolyte interface. [21] Formation of such electric double layer is clearly supported also by the MOF-DC based symmetric supercapacitor configuration fabricated with the same electrolyte solution (**Figure 6**). From the typical rectangular nature of cyclic voltammogram along with the charge-discharge profile, it is confirmed that the charge storage mechanism of the MOF-DC is a reversible non-faradic process.[44-46] The half-cell delivered the initial reversible capacity of ~66 mAh g^{-1} at current density of 150 mAh g^{-1}, which is almost two times higher than that of commercial AC (30-35 mAh g^{-1}) under Similar testing

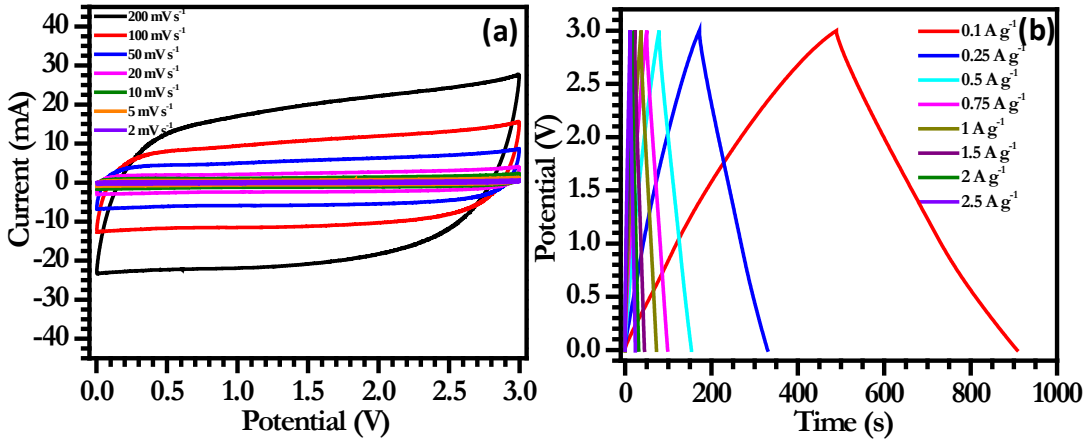

Figure 6(a) Cyclic voltammogram of MOF-DC based symmetric supercapacitor in the presence of 1 M LiPF6 in EC/DMC solution tested between 0-3 V at various scan rates. Each electrode is composed on 4 mg active mass loading over stainless steel substrate, and (b) Typical galvanostatic charge-discharge profiles of MOF-DC/MOF-DC symmetric supercapacitor cycled at various current densities. The applied current density is based on total active mass loading (4+4=8 mg), for example 1 A g–1 corresponds to the applied current of 8 mA**.**

conditions.[29, 32, 33] The observed capacity can be converted into the specific capacitance by the following equation:

$$C\ (F\ g^{-1}) = \frac{i(A) \times t(s)}{3600 \times m(g)} = mAh\ g^{-1} \times \frac{3600}{dV(mV)}$$

where, i is applied current, t is discharge time, m weight of the active material and dV is testing potential window of the single electrode configuration (mV, 1600 mV). However,

the mentioned relation is valid only for the case of linear variation of voltage vs. Time.[21] The specific capacitance value as calculated from this above equation is found to be~149 Fg^{-1}. The observed specific capacitance value is considerably higher than the commercial AC reported in the literature which is mainly ascribed to the presence of a high density of micropores in the synthesized carbon matrix.[29, 32, 33, 47] Further, MOF-CD carbon was found to retain ~92% of initial capacitance after 1000 cycles (**Figure 5b**). This single electrode performance clearly suggests that MOF-DC represents a promising candidate to employ in a Li-HEC configuration as cathode active material to achieve high energy density. Based on the electrochemical performance of both, the MOF-DC and the insertion anode $Li_4Ti_5O_{12}$, in single electrode configuration at the same current density (**Figure 7**), the mass loading between the anode to the cathode was fixed to 1:2.6 (3:7.8 mg) for the construction of Li-HEC.

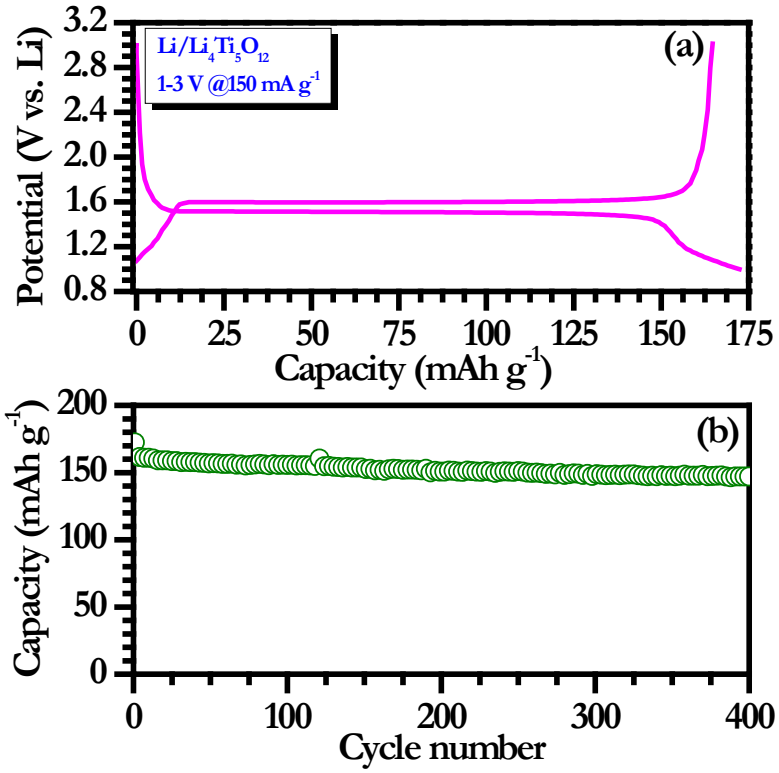

Figure 7 (a) Galvanostatic charge-discharge curves of $Li/Li_4Ti_5O_{12}$ (Sigma-Aldrich, USA) half-cells cycled between 1-3 V at constant current density of 150 mA g^{-1}, and (b) Plot of discharge capacity *vs.* cycle number.

Electrochemical profiles of MOF-DC/$Li_4Ti_5O_{12}$ Li-HEC were obtained between 1-3 V at various current densities and the results are illustrated in **Figure 8**. It is worth mentioning that the applied current densities were calculated based on the total active mass loading of 10.8 mg; for example, at the current density of 1 A g^{-1}, 10.8 mA current was applied to Li-HEC. It is apparent to note that increasing current density leads to decrease in the reaction time. This is mainly due to the partial participation of the active material in the electrochemical reaction, particularly Li-insertion/extraction in/from the spinel lattice.

As far as the charge storage mechanism is concerned, at the time of charging Li-ions present in the electrolyte solutions are intercalated into $Li_4Ti_5O_{12}$ lattice by the Faradic process, and in order to maintain the charge neutrality in the electrolyte, PF_6^- anions

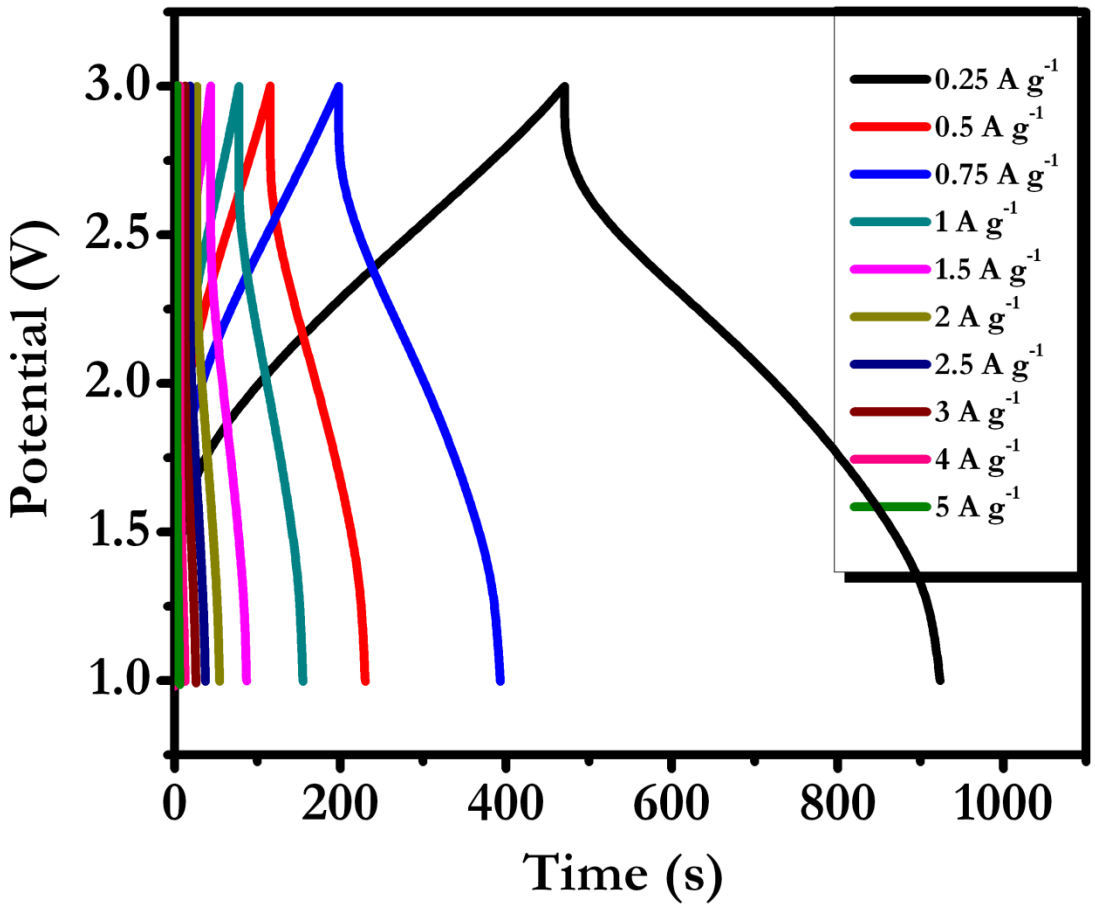

Figure 8 Galvanostatic charge-discharge curves of Li-HEC (MOF-DC/Li4Ti5O12) at various applied current densities.

adsorbed on the surface of MOF-DC, which eventually lead the formation of electric double layer (anion double layer) via non-Faradic process. The said reaction is reversed during discharge process. Specific energy (ESP) and power densities (PSP) are calculated according to the following equation, $P_{SP} = (E \cdot i / M)$ and $E_{SP} = (P_{SP} \cdot t)$, where $E = (E_{max} + E_{min})/2$; and , where ; E_{max} and E_{min} are the potential at the beginning and the end of discharge curves during galvanostatic measurements, respectively. M is the total active mass of both electrodes (10.8 mg). Based on the results and calculations, our MOF-DC/$Li_4Ti_5O_{12}$ Li-HEC is found to be capable of delivering maximum energy density of ~65Wh kg^{-1}(**Figure 9a**) which is significantly higher than commercial AC based Li-HEC fabricated with the same insertion anode (~36 Wh kg^{-1}) and the MOF-DC based symmetric supercapacitor configuration (~20 Wh kg^{-1}).

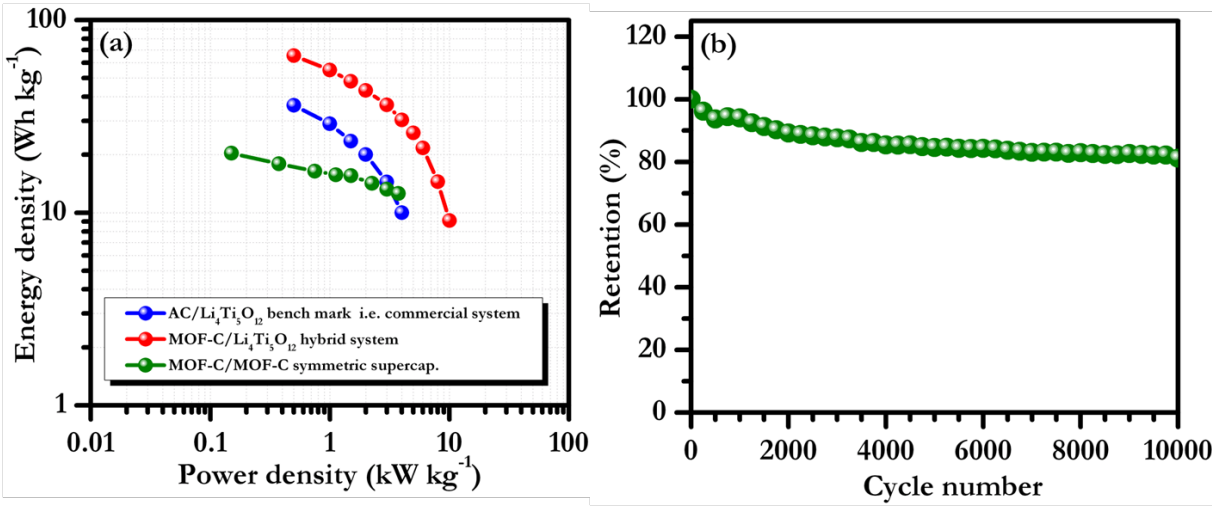

Figure 9 (a) Ragone plot and cycling profiles of MOF-DC/Li4Ti5O12 Li-HEC. (b)The Cycling profiles data points were collected after every 100 cycles.

Stoller et al. [48] first reported the performance of activated graphene with spinel phase $Li_4Ti_5O_{12}$ anode and presented an energy density of 40.8 Wh kg^{-1}. Higher energy density of ~45 Wh kg^{-1} was noted for the trigol reduced graphene oxide with appropriate mass loading and without any activation, as reported by us.[49] The observed values are very close to the maximum value (69 Wh kg^{-1}) for such Li-HEC configuration fabricated with different coconut shell derived porous carbons (36-69 Wh kg^{-1}) by our group.[47]

The MOF-DC is not only seen to outperform in terms of the energy density and but also in terms of the power capability of the system. This clearly suggests an excellent electrochemical performance of MOF-DC in Li-HEC configuration as cathode active material. The observed values are significantly higher than what is required to drive HEV applications (7.3-8.3 $Whkg^{-1}$).[20] Nevertheless, further improvements are anticipated to drive P-HEV (57 to 97 $Whkg^{-1}$) and EV (min 150 Wh kg^{-1}) applications.

Cyclability is another important parameter to ensure the viability of Li-HEC in real applications. In this regard, a duplicate Li-HEC was fabricated and subjected to long-term cycling at a current density of 2 A g^{-1}. The observed energy density (~30 Wh kg^{-1}) is normalized and illustrated in **Figure 9b**. Meager fading is noted during the prolonged cycling of 10000 cycles, which is mainly associated with the commercially available insertion anode $Li_4Ti_5O_{12}$.However, such fading can be improved by decorating the $Li_4Ti_5O_{12}$ particles with carbonaceous materials or making carbon composites as suggested by Naoi and co-workers [23-28]. The MOF-DC/Li4Ti5O12 Li-HEC is seen to retain ~82% of initial value (~25 Wh kg^{-1}) after 10000 galvanostatic cycles under harsh conditions. This clearly shows that MOF derived porous carbons is a highly promising material to construct high performance electrochemical energy storage devices. We attribute such exceptional performance to the unique crumpled-sheet assembled porous morphology endowed with very high surface area and the desired levels of micro and mesoporosity.

3.6 Conclusion

In conclusion, a very high surface area (2714 m^2 g^{-1}) carbon was synthesized by pyrolysing the zinc based metal organic framework (MOF-5) which exhibits unique crumpled-sheet assembled porous morphology with the desired levels of micro and mesoporosity. The supercapacitance behavior was investigated in single electrode configuration (vs. Li) in organic medium and a maximum specific capacitance of ~149 F $g^{-1}$was delivered with excellent cyclability. Such MOF derived carbon was then employed as cathode in Li-HEC with spinel phase insertion anode $Li_4Ti_5O_{12}$. The MOF-DC based Li-HEC delivered a maximum specific energy density of ~65 Wh k g^{-1} with an excellent power capability. Moreover, the MOF-DC based Li-HEC exhibited outstanding

cyclability (10000 cycles) and retained ~82% of initial value. This MOF based approach certainly opens a new platform for the development of high energy density electrochemical energy storage devices without compromising the power capability.

3.7 References

[1] R. J. Kuppler, D. J. Timmons, Q.-R. Fang, J.-R. Li, T. A. Makal, M. D. Young, D. Yuan, D. Zhao, W. Zhuang, H.-C. Zhou, Coord. Chem. Rev., **2009**, 253, 3042-3066.

[2] S. L. James Chem. Soc. Rev., **2003**, 32, 276-288.

[3] J. L. C. Rowsell, O. M. Yaghi, Angew. Chem. Int. Ed., **2005**, 44, 4670-4679.

[4] L. E. Kreno, K. Leong, O. K. Farha, M. Allendorf, R. P. Van Duyne, J. T. Hupp, Chem. Rev., **2011**, 112, 1105-1125.

[5] J.-R. Li, J. Sculley, H.-C. Zhou, Chem. Rev., **2011**, 112, 869-932.

[6] R. B. Getman, Y.-S. Bae, C. E. Wilmer, R. Q. Snurr, Chem. Rev., **2011**, 112, 703-723.

[7] A. Banerjee, R. Gokhale, S. Bhatnagar, J. Jog, M. Bhardwaj, B. Lefez, B. Hannoyer, S. Ogale, Journal of Materials Chemistry, **2012**, 22, 196 94-19699.

[8] F. Meng, Z. Fang, Z. Li, W. Xu, M. Wang, Y. Liu, J. Zhang, W. Wang, D. Zhao, X. Guo, Journal of Materials Chemistry A., **2013**, 1, 7235-7241.

[9] C. Hou, Q. Xu, L. Yin, X. Hu, Analyst, **2012**, 137, 5803-5808.

[10] X. Xu, R. Cao, S. Jeong, J. Cho, Nano Lett., **2012**, 12, 4988-4991.

[11] A. Banerjee, V. Aravindan, S. Bhatnagar, D. Mhamane, S. Madhavi, S. Ogale, Nano Energy., **2013**, 2, 890-896.

[12] A. Banerjee, U. Singh, V. Aravindan, M. Srinivasan, S. Ogale, Nano Energy, **2013**, 2, 1158-1163.

[13] S. J. Yang, T. Kim, J. H. Im, Y. S. Kim, K. Lee, H. Jung, C. R. Park, Chem. Mater., **2012**, 24, 464−470

[14] P. Pachfule, B. P. Biswal, and R. Banerjee, Chem. Eur. J., **2012**, 18, 11399 – 11408.

[15] P. Pachfule, V. M. Dhavale, S. Kandambeth, S. Kurungot, R. Banerjee, Chem. Eur. J., **2013**, 19, 974 – 980

[16] W. Chaikittisilp, M. Hu, H. Wang, H.-S. Huang, T. Fujita, K. C. W. Wu, L.-C. Chen, Y. Yamauchi, K. Ariga, Chem. Commun., **2012**, 48, 7259-7261.

[17] B. Liu, H. Shioyama, T. Akita, Q. Xu, J. Am. Chem. Soc., **2008**, 130, 5390-5391.

[18] J. Hu, H. Wang, Q. Gao, H. Guo, Carbon, **2010**, 48, 3599-3606.

[19] D. Yuan, J. Chen, S. Tan, N. Xia, Y. Liu, Electrochem. Commun., **2009**, 11, 1191-1194.

[20] E. J. Cairns, P. Albertus, Annual Review of Chemical and Biomolecular Engineering, **2010**, 1, 299-320.

[21] G. G. Amatucci, F. Badway, A. Du Pasquier, T. Zheng, J. Electrochem. Soc., **2001**, 148, A930-A939.

[22] I. Plitz, A. Dupasquier, F. Badway, J. Gural, N. Pereira, A. Gmitter, G. G. Amatucci, Appl. Phys. A., **2006**, 82, 615-626.

[23] K. Naoi, W. Naoi, S. Aoyagi, J.-i. Miyamoto, T. Kamino, Acc. Chem. Res., **2012**, 46, 1075-1083.

[24] K. Naoi, S. Ishimoto, J.-i. Miyamoto, W. Naoi, Energy & Environmental Science. , **2012**, 5, 9363-9373.

[25] K. Naoi, Y. Nagano in Li-Ion-Based Hybrid Supercapacitors in Organic Medium, Vol., Wiley-VCH Verlag GmbH & Co. KGaA, **2013**, pp.239-256.

[26] K. Naoi, P. Simon, Electrochem. Soc. Interface., **2008**, 17, 34-37.

[27] K. Naoi, Fuel Cells, **2010**, 10, 825-833.

[28] K. Naoi, S. Ishimoto, Y. Isobe, S. Aoyagi, J. Power Sources., **2010**, 195, 6250-6254.

[29] V. Aravindan, W. Chuiling, M. V. Reddy, G. V. S. Rao, B. V. R. Chowdari, S. Madhavi, PCCP., **2012**, 14, 5808-5814.

[30] V. Aravindan, M. V. Reddy, S. Madhavi, G. V. S. Rao, B. V. R. Chowdari, Nanoscience and Nanotechnology Letters, **2012**, 4, 724-728.

[31] V. Aravindan, M. V. Reddy, S. Madhavi, S. G. Mhaisalkar, G. V. Subba Rao, B. V. R. Chowdari, J. Power Sources, **2011**, 196, 8850-8854.

[32] V. Aravindan, N. Shubha, W. C. Ling, S. Madhavi, Journal of Materials Chemistry A., **2013**, 1, 6145-6151.

[33] V. Aravindan, W. Chuiling, S. Madhavi, J. Mater. Chem., **2012**, 22, 16026-16031.

[34] V. Aravindan, Y. L. Cheah, W. F. Mak, G. Wee, B. V. R. Chowdari, S. Madhavi, ChemPlusChem. , **2012**, 77, 570-575.

[35] L. Cheng, H.-q. Li, Y.-y. Xia, J. Solid State Electrochem., **2006**, 10, 405-410.

[36] H. Kim, M.-Y. Cho, M.-H. Kim, K.-Y. Park, H. Gwon, Y. Lee, K. C. Roh, K. Kang Advanced Energy Materials., **2013**, 3, 1500-1506.

[37] H. Li, M. Eddaoudi, M. O'Keeffe, O. M. Yaghi, Nature, **1999**, 402, 276-279.

[38] S. S. Kaye, A. Dailly, O. M. Yaghi, J. R. Long, J. Am. Chem. Soc., **2007**, 129, 14176-14177.

[39] F. Tuinstra, J. L. Koenig, The Journal of Chemical Physics, **1970**, 53, 1126-1130.

[40] A. C. Ferrari, D. M. Basko, Nature Nanotechnology, **2013**, 8, 235-246.

[41] A. C. Ferrari, J. Robertson, Phys. Rev. B: Condens. Matter., **2000**, 61, 14095.

[42] A. M. Rao, A. Jorio, M. A. Pimenta, M. S. Dantas, R. Saito, G. Dresselhaus, M. S. Dresselhaus, Phys. Rev. Lett., **2000**, 84, 1820-1823.

[43] V. Khomenko, E. Raymundo-Pinero, F. Beguin, J. Power Sources, **2006**, 153, 183-190.

[44] M. Inagaki, H. Konno, O. Tanaike, J. Power Sources, **2010**, 195, 7880-7903.

[45] A. G. Pandolfo, A. F. Hollenkamp, J. Power Sources, **2006**, 157, 11-27.